A SOLAR WIND DEUTERIUM DETECTOR AND CHARGE-SPECTRUM ANALYZER

by

Franklin W. Floyd, Jr.

A SOLAR WIND DEUTERIUM DETECTOR AND CHARGE-SPECTRUM ANALYZER

by

FRANKLIN WEAVER FLOYD, JR.

B.E.E., Georgia Institute of Technology
(1961)

SUBMITTED IN PARTIAL FULFILLMENT OF THE
REQUIREMENTS FOR THE DEGREE OF
MASTER OF SCIENCE
at the
MASSACHUSETTS INSTITUTE OF TECHNOLOGY
November, 1964

Signature of Author _____
Department of Electrical Engineering, November 30, 1964

Certified by _____
Thesis Supervisor

Accepted by _____
Chairman, Departmental Committee on Graduate Students

A SOLAR WIND DEUTERIUM DETECTOR AND CHARGE-SPECTRUM ANALYZER

by

FRANKLIN WEAVER FLOYD, JR.

Submitted to the Department of Electrical Engineering on November 30, 1964 in partial fulfillment of the requirements for the degree of Master of Science

ABSTRACT

13236
~~13246~~

A more complete knowledge of the chemical profile of the solar wind would reveal more clearly the nature of the high energy nuclear processes taking place on the surface of the sun.

An instrument for satellites or space probes is described which will measure the relative abundance in the solar wind of the hydrogen isotope, deuterium and possibly of the helium isotope, He^3. It will also reveal the relative abundances of certain light positive ions by measuring the charge-spectrum of the solar wind up through a positive charge of about eight times the proton charge.

A laboratory model of the instrument is described. The results of preliminary tests in vacuum show the concepts to be feasible. The results of these tests are discussed and suggestions are made for further development of the instrument.

Author

Thesis Supervisor: Frank Scherb
Title: Assistant Professor of Physics

ACKNOWLEDGMENT

I want to thank Professor Frank Scherb, who originally suggested this problem and furnished many of the references for the background material in the first chapter. I sincerely appreciate his continued interest and many helpful suggestions during the course of this work.

Franklin W. Floyd, Jr.

TABLE OF CONTENTS

Chapter I: Introduction

1.1 Background

The interplanetary plasma, or solar wind, as it is variously called, is the neutral plasma which streams continuously outward from the sun. It is actually a continuation of the solar atmosphere or corona. Its existence has been experimentally confirmed by several satellites, including the Mariner II space probe on its flight to Venus. Since then much effort has been spent in studying its nature in more detail. Several instruments have investigated the total flux as a function of energy for both positive and negative particles, but no one has yet attempted to probe into the composition of the plasma. Of course the vast majority of the positive ions are probably protons and the Mariner II results (S4) indicate that there may be as much as ten percent of helium present, but beyond this almost nothing is known about the chemical profile of the plasma. Isotopes other than H^1 and He^4 are almost certainly present in relatively small quantities (S3). A more complete knowledge of which elements and isotopes are present in the plasma and their relative abundances would shed considerable light on many important astrophysical problems concerning stellar processes in general and in particular about our own sun.

This thesis will mainly be concerned with detecting the hydrogen isotope, deuterium (D). An experiment has been proposed by Dr. F. Scherb of the M.I.T. Laboratory for Nuclear Science by which the relative abundance of D and possibly of He^3 can be measured and by which the charge spectrum of the plasma can be determined up to a positive charge of about eight times the proton charge. A laboratory model of this experiment was constructed and tested in a simulated space environment. Results of these preliminary tests indicate that the technique is feasible. While the experiment presents some unusual engineering problems, the work done so far has shown that these are certainly surmountable and should not unduly delay the development of a workable flight model once the project is undertaken. The construction of the laboratory model of the experiment will be described in detail in hope that some of the techniques which gradually evolved from the process of trial and error will be of use to those who continue the development of this first primitive model into an instrument suitable for space flight.

The procedures followed in testing the model are also described. These tests were done first to determine whether or not the concepts were even workable and then to begin accumulating the data and experience upon which a reasonable design and set of specifications for an actual instrument could be based.

1.2 Relative Abundance of the Elements

Traditionally there have been three methods for studying the relative abundance of the different elements in the universe: (1) direct chemical analysis of terrestrial and meteoritic material, (2) analysis of cosmic rays, and (3) spectroscopic analysis of radiation from stars (especially the sun) and nebulae. Recently the techniques of radio astronomy have also been used in investigation of element abundances.

The isotope deuterium has been observed only on earth and in meteoritic material where its abundance relative to ordinary hydrogen is about 1.4×10^{-4}. There have been a number of attempts to detect the presence of deuterium on the solar surface based on the isotope shift in the spectral lines of deuterium relative to hydrogen (S3), particularly in the Dα line which, at 6561Å, is 1.8Å on the blue side of the Hα line. The result that deuterium was not observed in these investigations places an upper limit of about 10^{-4} on its abundance relative to hydrogen. Kinman (K1) reported that his investigation would have detected deuterium if its relative abundance had exceeded 4×10^{-5}.

The actual abundance of deuterium on the solar surface may well be much less than this. It is continuously produced in the core of the sun by the thermonuclear reaction,

$$p + p \longrightarrow D + \beta^{+} + \nu \qquad (1\text{-}1)$$

but is also consumed by the much more rapid reaction,

$$D + p \longrightarrow He^3 + \gamma \qquad (1\text{-}2)$$

so that its relative abundance in the solar core is only about 10^{-17}.

Based on equilibrium thermonuclear reactions only, an estimate of the relative abundance of deuterium on the solar surface could range from 10^{-17}, the abundance in the solar core, to an uncertain upper limit of about 10^{-5}, slightly less than its abundance on earth.

If deuterium were present on the surface of the sun, then convective circulation would probably carry it down to a depth where the temperature is high enough for reaction (1-2) to occur. Greenstein and Richardson (G3) estimated the temperature at the bottom of the convection zone to be between 2×10^{-6}°K and 3×10^{-6}°K. This was based on the observation (G4) that the relative abundance of beryllium on the sun is about the same as on earth whereas that of lithium is lower by a factor of 50. If the original abundance of deuterium on the solar surface were comparable to that presently on earth (1.4×10^{-4}), then a temperature of only 0.54×10^{6}°K (S2) would be sufficient to have completely destroyed it by reaction (1-2) within the estimated lifetime of the sun (5×10^{9} yrs), so this evidence indicates that deuterium should be essentially nonexistent on the solar surface if there has been no production of more deuterium on the surface

since the sun formed. The fact that there is some lithium remaining on the surface, however, indicates that the convective process may be relatively slow. Greenstein and Richardson (G3) estimate that the characteristic time for material to circulate in the convective region is 7×10^8 years or one seventh of the estimated lifetime of the sun. P. Morrison (M2), however, has commented that while convection undoubtedly exists, its rate is not known as it is probably influenced by subsurface magnetic fields about which little is known. The present evidence, however, seems to indicate that any deuterium present when the sun was formed has long since been consumed to produce He^3.

These considerations reflect on the larger astrophysical problem of the relative abundances of the nuclear species D, Li, Be, and B which are all produced in stellar thermonuclear reactions, but which are quickly consumed by further reactions so that their observed abundances in the universe cannot be explained in terms of thermal processes, although these processes are thought to account for the observed abundances of many of the other elements (B3).

Burbidge, et al. (B3) have considered the possibility that flare activity may provide the necessary nonthermal processes by bombarding the stellar surfaces with high-energy particles leading to the formation of D, Li, Be, and B through spallation of heavier elements, or by

neutron capture. Indeed, Goldberg et al.(G1) reported that spectroscopic observation of a solar flare which occurred on February 10, 1956, indicated a possible deuterium concentration of 5 to 10% although this result was not confirmed by other observers.

Fowler, Greenstein, and Hoyle (F1) suggest that D, Li, Be, and B in the inner solar system may be the residual products of large scale flare activity during the early history of the sun. In their theory the local abundances of these isotopes reflect only on the history of the solar system and may be quite different from any "universal" abundance for the galaxy.

Heller (H1) considered the production of D by supernovae explosions. He concluded that under certain conditions enough D could be produced and preserved in a localized region to account for its observed relative abundance on earth, but his theory would not explain this same abundance throughout the galaxy.

1.3 The Solar Wind

Recent observations of the solar wind show a particle flux of several times 10^8 particles $cm^{-2}sec^{-1}$ and an average velocity ranging from 300 to 800 km sec^{-1} (S4). Satellites and space probes now offer a means, as yet unexploited, for obtaining information on the relative abundance of elements on the surface of the sun through analysis of the solar wind.

One technique for analyzing the constituents of the solar wind would be the use of electric and/or magnetic fields in a spectrometer or time-of-flight configuration. Aside from problems of size and weight of the apparatus, this technique has the disadvantage that it is sensitive only to the ratio of charge-to-mass. It would be very difficult to build an instrument suitable for space application which would resolve, for instance, D^+ and He^{++} whose charge-to-mass ratios differ by only 0.7%.

It is desirable to distinguish D^+ from the other components of the solar wind because of its direct bearing on the astrophysical questions mentioned in the last section. The techniques described here will allow an accurate determination of the relative abundance of deuterium in the solar wind if the abundance exceeds about 10^{-5} and, by means of a charge spectrum analysis, will provide considerable insight into the relative abundances of other light elements in the solar wind.

Chapter II: The Proposed Experiment

2.1 Deuterium Detector

The technique proposed for detecting the presence of deuterium in the solar plasma makes use of the exoergic nuclear reaction between deuterium and tritium,

$$D + T \longrightarrow He^4 + n + 17.6 \text{ Mev.} \qquad (2.1)$$

The resulting alpha particle and neutron have unique energies of 3.6 and 14 Mev respectively. The cross-section for this reaction, plotted as a function of deuteron energy in Fig. 1, has a strong resonance at a deuteron bombarding energy of about 100 Kev.

The proposed instrument would sample the solar plasma through an entrance grid several inches in diameter. Upon passing through this grid, the positive ions in the plasma would be accelerated through a potential difference of about 100 kilovolts and focused upon a tritiated target of the type commonly used for producing neutrons by the above reaction. A certain percentage of the D^+ ions would produce 3.6 Mev alpha particles by reaction (2.1). A measurement of the alpha production rate then indicates the amount of deuterium present in the plasma. The alpha particles are in the range of energy that can be detected very conveniently by a solid state radiation detector located immediately adjacent to the target. Being practically monoenergetic, they would permit rather strong discrimination against extraneous events.

A detector of the surface barrier type would be the most suitable for this application.

An estimate of the counting rate obtained by this technique can be made from the data published by Gunnersen and James (G5), who measured the efficiency of reaction (2.1) in titanium tritide targets. Using a typical target with 1.5 tritium atoms per titanium atom, they obtained yields of 1×10^{-6} He^4 per D at 80 Kev of deuteron energy and 2.5×10^{-6} He^4 per D at 100 Kev. Assuming a solar wind positive ion flux of 5×10^8 particles $cm^{-2} sec^{-1}$ (S4), a deuterium relative abundance of 10^{-5}, and an entrance grid of 100 cm^2, the corresponding alpha production rates are 1.1 sec^{-1} at 100 Kev and 0.7 sec^{-1} at 80 Kev. By careful placement of one or more solid state detectors, probably 30 percent of these alphas could be detected.

2.2 Sources of Natural Background

The estimate in the last section indicates that an instrument of this type will have, at best, a counting rate of a few counts per second. Its sensitivity will be determined almost entirely by the background counting rate.

A survey was conducted of other ions possibly existing in the solar plasma to determine if any of them could cause an ambiguity by producting events in the

target which could be confused with the deuterium-tritium events. One possible source of trouble is the isotope, He^3, which may be present due to the rapid conversion of deuterium to He^3 in the sun by reaction (1.2). The reaction between He^3 and tritium has three possible final states:

$$(43\%) \quad He^3 + T \longrightarrow He^4 + D + 14.3 \text{ Mev} \qquad (2.2a)$$

$$(51\%) \quad He^3 + T \longrightarrow He^4 + n + p + 12.1 \text{ Mev} \qquad (2.2b)$$

$$(\ 6\%) \quad He^3 + T \longrightarrow He^5 + p + 14.1 \text{ Mev} \qquad (2.2c)$$

$$\hookrightarrow He^4 + n$$

The total cross section for the He^3-tritium reaction is shown in comparison with the D-T cross section in Fig. 1. It is seen to be smaller by a factor of 1000 than the deuterium-tritium cross section.

Reaction (2.2a) produces deuterons and alphas with discrete energies of 9.55 Mev and 4.75 Mev respectively. These should be easily distinguishable from the 3.6 Mev alphas due to deuterium. Indeed, this reaction can be regarded as a means for measuring the abundance of He^3 in the solar wind. Because of its relatively small reaction cross section, He^3 would have to be present in an abundance 1000 times greater than that of deuterium to produce a comparable counting rate. Such a high relative abundance of He^3 cannot be ruled out at present. The only available information on its abundance on the sun is due to Greenstein who searched for evidence of it in the solar

spectrum. He did not find a positive indication of the presence of He^3 and placed an upper limit of 2% on its abundance relative to He^4(G2).

Reactions (2.2b) and (2.2c) are potentially a more serious source of background than reaction (2.2a) because they produce alphas and protons which do not have unique energies. Some of these particles could then have the same energy as the deuterium-produced alphas. If the abundance of He^3 is determined from reaction (2.2a), however, a statistical correction can be made in the data to account for the background due to reactions (2.2b) and (2.2c). It should be possible to distinguish further between the deuterium reactions and the He^3 reactions by studying the counting rate as a function of accelerating potential. The deuterium-tritium cross section increases by only ten percent from 90 to 110 Kev while that of the He^3-tritium reaction increases by a factor of two. In fact, for voltages above 100 Kv the energy dependence of the He^3-tritium reaction is quite different from that of the deuterium-tritium reaction (see Fig. 1).

The tritium target itself is another potential source of background which must be investigated. The amount of tritium is such that there will be about 10^{10} beta disintegrations per second and possibly as

many as 10^5 bremsstrahlung x-rays per second. The individual events would be insignificant, but there is a possibility of false counts due to pile-up. The preliminary laboratory results show that the target activity does cause a slight decrease in resolution, but a false event due to pile up has never been observed. Consequently, the target activity does not appear at this time to be a serious problem.

Cosmic rays are another source of background, but their effect on this type of instrument is difficult to estimate. Since solar flares occasionally are copious sources of high energy particles (S3), measurements of deuteron fluxes made during and after such events will be very valuable due to the possible production of deuterium on the solar surface by such flare activity. After a tentative design has been chosen for the instrument package, it will be necessary to investigate further the background effect of high energy flare particles incident on the space vehicle.

In many flare events the high-energy particle flux returns almost to pre-flare levels before the bulk of the low energy plasma particles reach the vicinity of the earth's orbit (S3) (B4). For these events the solar plasma associated with a flare may be analyzed for deuterium after the energetic particle flux has subsided.

2.3 Charge Spectrum Analysis of the Plasma

In addition to the detection of deuterium and the possible detection of He^3, the 100 kilovolt accelerating potential makes it possible, with only a small increase in instrumental complexity, to measure the relative amounts of certain positive ions. This can be done by adding another solid state detector at the negative 100 kilovolt potential. It would be positioned so that a small sample of the flux of incoming particles would fall upon its sensitive surface. Each of these particles would produce a signal proportional to its total kinetic energy. If all ions present in the solar wind are assumed to have an average velocity near the observed bulk velocity for the plasma which is 300 to 800 Km sec^{-1} (S4), then (neglecting the comparatively small thermal velocities) the average kinetic energy per particle would be between 0.5 and 4 Kev for protons, 2 to 16 Kev for He^4, and 4 to 32 Kev for oxygen.

The additional energy imparted to a positive ion by the 100 kilovolt potential is proportional to the charge of the ion and should, in all cases, be much greater than the original energy of the ion because there is reason to believe that all of the lighter elements present in the plasma are essentially completely ionized (S3). Therefore each particle reaching the detector will have an energy which is very nearly proportional to its

(positive) charge. Thus pulse height analysis of the detector output will reveal the charge spectrum of the plasma.

Solid state detectors are light-sensitive devices. Since the detector for charge spectrum analysis will be facing into the line of flight of the incoming particles, there is no way to shield it absolutely from sunlight at all times unless a deflection field is used to bend the trajectory of the particles. Fig. 2 , however, shows that the detector need not be facing in the direction of the sun to take data. Thus, by focusing the particle beam through a small aperture, the effect of sunlight should be essentially eliminated except at times when the attitude of the spacecraft is such that the detector is looking directly at the sun, at which times the detector can simply be gated off.

With an average solar wind particle flux of several times 10^8 particles cm^{-2} sec^{-1}, the only problem concerning the counting rate of the charge spectrum analyzer is to keep it from exceeding the signal processing capacity of the circuits. A desired counting rate should be realizable by proper geometric design and beam focusing.

2.4 Instrument Design Factors

Figure 2 shows, in block diagram form, what the physical configuration of the instrument might be like.

Conceptually the experiment itself is not complicated. Certainly the electronic instrumentation will not be too complex as space experiments go, but the high voltage required for this experiment plus the fact that it must be vacuum insulated will make the structural design quite a difficult problem both electrically and mechanically. Indeed, the high-voltage power supply and the beam focusing structure together will probably represent the major part of the effort required to develop and build a workable model of the experiment.

Another problem is that of coupling the electronic signal out through the 100 Kv potential difference. Gallium arsenide diodes were used to produce an amplitude-modulated infrared light beam for signal coupling in the laboratory model of the instrument and it appears that this technique will provide a convenient solution to the signal-coupling problem in future models.

Referring again to Fig. 2, the focusing field is formed by two concentric metal shells, each in the form of a hemisphere joined to a cylinder. The outer shell is at satellite ground potential and contains the entrance grid in its hemispherical portion. The inner shell is at a negative potential of about 100 kilovolts with respect to satellite ground. Upon entering through the grid, the positive ions in the plasma are accelerated and focused into a converging conical beam by the radial

electric field in the gap between the hemispherical surfaces. Upon reaching the inner shell, a fraction of the particles pass through a grid in its hemispherical surface and converge to the center of curvature of the hemispheres. At its point of maximum convergence the beam passes through a small aperture which excludes most of the incident sunlight. The beam then diverges slightly to be uniformly distributed over the target surface (a small segment bypasses the tritium target and falls directly upon the charge spectrum analyzer). The solid state detector is arranged to intercept the maximum number of deuterium produced alpha particles without interfering with the incoming ion beam.

In the present concept, the deuterium detector and charge spectrum analyzer each has its own separate and independent measurement chain consisting of preamplifier, amplifier, and infrared signal transmitter. However, since power for operating the circuits inside the high potential shell will be at a premium, it may prove advantageous to allow parts of the circuitry to serve both instruments by switching modes of operation either automatically or on command. The problem of supplying power to the circuits inside the high potential shell has not yet been considered in detail. In the laboratory model of the experiment a 6 volt mercury cell was used to supply the 30 mw of power required for these circuits.

The high-voltage power supply and supporting insulators are mounted well back from the hemispherical surface of the shell to minimize their perturbing effect on the radial focusing field. The power supply itself is mounted in the rear of the cylinder and in line with its axis. The work done so far in developing a power supply suitable for space application indicates that a unit can be built with sufficient mechanical strength to support its own weight and provide part of the support for the high potential shell, especially in the axial direction.

This completes the description of the principles of operation of the instrument and proposed concept for its construction. The details of signal processing, logic, memory, control, etc. will not be discussed here as they are all fairly routine matters in the instrumentation of space experiments and can best be considered in detail in relation to a specific mission for the experiment.

Chapter III: A Prototype Model

The major part of the experimental work on which this thesis is based consisted of building and testing a prototype model of the proposed instrument which simulated, as closely as practicable, the design concept outlined in the previous chapter. The primary objective of this work was to verify the feasibility of the concept and to make preliminary measurements of efficiency and resolution. In the interest of meeting this objective in a reasonable length of time, many of the design problems which appeared to require considerable developmental work could not be considered here. It should be stressed, therefore, that this work is not intended to represent a final design description.

3.1 High Voltage Power Supply

The standard Cockroft-Walton capacitor-diode circuit was chosen as the most appropriate method, in this case, for generating high DC voltage. The circuit used consists of eight capacitor-diode stages rated at 10 kilovolts DC per stage. It is driven by a 10 kilovolt peak-to-peak sinusoidal voltage at a frequency of 5 kc/sec. An oscillator and step-up transformer provide the driving voltage.

In its present form the supply is capable of providing a DC voltage of 80 kv. A shortage of components at the time the supply was built prevented the addition of two more stages necessary for 100 kv.

The capacitors used are unencapsulated barium titanate ceramics rated at 2200 pf, 10 kv DC (Sprague 706C3). These are small disc-shaped units and are stacked together alternately with disc-shaped aluminum corona shields to form a compact, self-supporting column (Fig. 4). The capacitor-diode network consists of two of these columns adjacent to one another with the diodes connected between the columns. The corona shields also serve as terminals for connecting the diode leads.

The diodes used are 16 kv units with axial wire leads. (Solitron MC4-16). These are overrated in voltage by 60 percent, but past experience showed that the diodes must be considerably overrated if they are to survive repeated surges.

The entire structure was encapsulated by dipping in silicone rubber potting compound (RTV-11). This was done in vacuum to eliminate the possibility of trapped gas bubbles in the encapsulating material.

The completed structure weighs 1089 grams. Much of this weight is due to the solid aluminum corona shields and could be reduced considerably by careful design. The approximate dimensions are 5 cm by 10 cm by 10 cm high. Figure 3 shows this power supply compared with an earlier model.

The power requirement (Fig. 13) is 3.4 to 3.7 watts at 80 kv depending on the pressure in the vacuum system

(4×10^{-5} to 3×10^{-6} Torr). Most of this power is due to the driver transformer which requires a large open circuit charging current. At 80 kv DC the ripple voltage is 1.8 kv or 2.2 percent.

The design and construction details are described more completely in Appendix A.

This power supply has given excellent service. Over the past two months it has been operated at 80 kv repeatedly in vacuum for periods of up to several hours. It has never suffered a voltage breakdown except when high-voltage breakdown in some other part of the vacuum system induced arcing along its outer surface. It can withstand repeated surges of this type, without the protection of a current-limiting circuit, and suffer no apparent ill effects.

Barium titanate, however, may prove to be unsuitable for an actual space application because it has some undesirable characteristics. Its dielectric constant (1200 at 40°C) is quite temperature sensitive. Mechanically, barium titanate is a hard, brittle substance which may chip or shatter under vibrational testing. These factors could easily negate the advantages it offers in design compactness and must be carefully evaluated in future designs. The possibility of using capacitors made of mica is presently being studied.

3.2 Ion Beam Focusing

The concept, outlined in the previous chapter, of two cylindrical shells with hemispherical ends is used in this prototype to provide a radial focusing field. The diameter of the outer (ground potential) shell is 12 inches, while the inner shell is 3 inches in diameter. The cylindrical portion of each of the shells is 6 inches long (Figs. 8 and 9).

The entrance grid in the outer shell is made of 64 percent transparent screen while the inner shell has a grid formed by holes drilled in its hemispherical surface. Its transparency is 26 percent.

The inner shell is supported by four lucite insulators. Since optimum focusing of the ion beam was not considered important in this prototype model, no provision was made to align the inner shell accurately and hold it in place. Separate equipment is presently being assembled to conduct a thorough study of particle trajectories and beam focusing with the radial field configuration.

At first the beam focusing structure would not maintain the 80 kv accelerating potential in vacuum. Breakdown occurred at voltages from 30 kv to 55 kv and was always preceded by these symptoms:

(1) a sharp increase in current to the power supply,

(2) a "limiting" effect on the high voltage,

(3) a diffuse glow which sheathed the insulators and electrode surfaces,

(4) occasional small points of intense light on the anode (outer shell) and sometimes in remote parts of the vacuum system,

(5) larger, less intense, areas of light around the base of the power supply and on the teflon sheet which supported it.

Once breakdown occurred, the vacuum system seemed to become contaminated as it was then impossible to raise the voltage at all until the system had been allowed to recover for several minutes.

The mechanisms which cause vacuum breakdown are not well understood. Breakdown strength becomes relatively independent of gap length for gaps larger than about 1 cm (D1). Recent evidence indicates that a rapid increase in ion exchange between positive and negative electrode surfaces generally precedes vacuum voltage breakdown (B2)(M1). Kofoid (K2) studied the effect of electron emission from the negative electrode-dielectric junction on the breakdown strength of insulators.

The breakdown voltage of the beam focusing structure was increased slightly by reducing the area of contact between the negative electrode (inner shell) and its supporting insulators. It was found, however, that a thin coat of dielectric material over the inside surface of the outer shell (anode) effectively eliminated the high voltage

breakdown problem -- at least up to 80 kilovolts. At first a sheet of teflon film was used and then a baked-on coat of Durafilm High Dielectric Enamel. The teflon performed well from the beginning, but the enamel required a period of outgassing and conditioning by repeated arcing before its performance matched that of teflon.

This technique is not proposed here as a final solution to the high-voltage problem. The purpose of the hemispherical portion of the outer shell is to define a radial field for beam focusing, and covering it with a film of dielectric tends to defeat this purpose. However if further investigation shows that the field is not seriously perturbed by the dielectric film, then this could prove to be quite a valuable technique.

3.3 Electronics

The deuterium detection and charge spectrum analysis portions of the experiment were tested separately. This was done to avoid the time-consuming job of laying out and packaging both circuits to fit together inside the inner shell.

The same electronics package, with minor modifications, was used to test both parts of the experiment. Figure 6 shows the package adapted for testing the deuterium detector. Included in the package are the preamplifier, two stages of voltage amplification, one stage of current

amplification and a gallium arsenide infrared light source for transmitting the signals to a photomultiplier tube at ground potential.

Because the capacitance of solid state detectors is sensitive to ambient conditions, it is a standard technique to use a "charge sensitive" preamplifier with them. Referring to Fig. 7, the preamplifier consists of the two cascode-connected input transistors (Q_1 and Q_2) which drive an emitter-follower output stage (Q_3). Capacitive feedback (C_1) from the emitter of Q_3 to the base of Q_1 (input) produces the "charge sensitive" feature. Transistor pairs Q_4-Q_5 and Q_6-Q_7 form two identical stages of voltage amplification, each with negative feedback. Transistors Q_8 and Q_9 provide the current amplification necessary to drive the infrared source. Capacitors C_2 and C_3 shape the system frequency response by providing equal integrating and differentiating time constants of one microsecond each.

The total gain of the system can be expressed in terms of the infrared diode pulse current per Kev of energy (of a particle incident on the solid state detector). For operation as a charge spectrum analyzer, the system gain is adjusted to 0.1 ma per Kev and for the deuterium detector it is about .03 ma per Kev.

The infrared source (Texas Instruments SNX-100) is forward biased at three milliamps which is sufficient

to make its response essentially linear. This bias current is not temperature-stabilized in the present model. The power requirement of the entire circuit is 5 ma at 6 volts. This is provided by a mercury cell sealed in a vacuum-tight container (see Fig. 6).

Manufacturer's specifications indicate that the infrared source emits about 0.44 microwatts of optical power per milliamp of junction current at 25°C. This figure increases rapidly for lower temperatures. A measurement of the radiation pattern showed that the half-power beam width is 43 degrees. The optical response to a current step of 10 milliamps was measured with a photomultiplier tube and showed a rise time of about 0.5 microseconds. Much faster response has been obtained at higher current levels.

The preamplifier and infrared transmission system are discussed in more detail in Appendix B.

In this model of the experiment the infrared light signal is beamed directly to a photomultiplier tube at ground potential. A signal transmission system was built, however, which uses a solid state particle detector as the infrared sensor. A dielectric light pipe is used to guide the infrared beam to the sensitive surface of the detector. This technique will be studied in more detail, but it appears likely that it will allow the phototube to be eliminated in future models of the experiment. This subject is discussed further in Appendix B.

The resolution of nuclear particle detection systems is usually specified in terms of the full-width-at-half-maximum (FWHM) spread, due to system noise, in the output spectrum. This figure is given in units of energy referred to the system input. The noise performance of charge-sensitive preamplifiers for solid state particle detectors is degraded by adding external capacitance to the input terminals. The relationship between noise and external capacitance is expressed as a function of capacitance by a straight line whose slope (in Kev FWHM per pf) and intercept (in Kev FWHM) at zero external capacitance are specified. The amplifier built for this experiment has a FWHM noise of 20 Kev at zero capacitance and a slope of about .13 Kev per pf. These figures do not account for the noise contribution of the detector itself, only the degradation in amplifier performance caused by the capacitance of the detector. The infrared signal transmission system did not contribute appreciably to the noise of the system.

3.4 Charge Spectrum Analyzer

The proposed technique of charge spectrum analysis was tested with a small-area, low-capacitance, high-resolution detector well suited for low-energy particle detection (Ortec # 4-755A).

Its resolution for protons was specified as 10 Kev FWHM at a bias of 25 volts. In this model of the

experiment the detector is biased at only 4 volts by using the 6 volt mercury cell which powers the amplifier. Its capacitance at 4 volts bias is 80 pf which increases the amplifier noise from 20 to 29 Kev FWHM. The total noise of the system, including detector, was measured and found to be 36 Kev FWHM. The methods of calibration and noise measurement are discussed in Appendix A.

It is apparent that the preamplifier is the dominant contributor to the system noise. Since it would be desirable to improve the system noise performance, a preamplifier using a field-effect transistor as its input stage is being developed for use in the charge spectrum analysis system.

For these tests the detector was mounted on the front of the electronics package in the position occupied by the tritium target holder in the photograph (Fig. 6). No means for controlling the counting rate, such as the light baffle and aperture discussed in the previous chapter, was included in this model of the experiment. To reduce the particle flux incident on the detector to a reasonable value, it was therefore necessary to seal off all but one hole of the grid in the surface of the inner shell.

3.5 Deuterium Detector

Figure 6 shows the electronics package with the tritium target and solid state detector mounted. The

detector used for this test was a 300 mm^2 device with a specified resolution of 90 Kev FWHM for alpha particles (Ortec # 4-815). The large area was necessary in this case to intercept as many of the deuterium-produced 3.6 Mev alpha particles as possible.

This detector was also biased at four volts. The depletion depth for this voltage is 90 microns which should completely stop alpha particles with energies up to about 12 Mev.

Chapter IV: Testing and Evaluation

4.1 Experimental Procedure

Figure 8 is a block diagram of the laboratory set-up used for testing and evaluating the prototype model. Tests were carried out in vacuum at pressures of from 4×10^{-5} to 3×10^{-6} Torr. The ion beam was produced by a Vacuum Electronics Corporation Veetube ion source. A deflecting magnet in the ion source allowed selection of the charge-to-mass ratio of the beam. For testing the deuterium detector a palladium leak introduced controlled quantities of hydrogen or deuterium gas into the ion source. The ion beam produced by residual gas in the vacuum system was sufficient for testing the charge spectrum analyzer.

Ion beam intensity was measured with a Faraday cup which could be lowered into the beam path by means of a sliding seal. Figures 10 and 11 show the ion beam current as a function of ion source accelerating potential (0-1000 v). The strong peaks in beam current correspond to different values of charge-to-mass ratio.

As explained in the previous chapter, the pulses from the particle detector were transmitted by an infrared light beam from the inner shell at 100 kv potential to a phototube at ground potential. The phototube output was amplified by one emitter-follower stage before passing out of the vacuum system. A multi-channel pulse height analyzer (100 to 400 channels),

oscilloscope, and pulse counter were used to analyze the output signals.

The accelerating potential was measured with a resistor voltage divider consisting of two 30 kv, 10^{11}ohm RPC carbon film resistors connected in series with a two-megohm resistor for a divider ratio of 10^5:1. The divider output was measured with a high impedance vacuum tube voltmeter. The divider was accurate to within two percent up to 30 kv, but could not be calibrated at higher voltages. The high voltage was controlled by adjusting the input voltage to the driver circuit.

4.2 Resolution of the Deuterium Detector

One of the assets of this method of deuterium detection is that the unique energy of the alpha particle allows strong discrimination against extraneous events. It was of interest, therefore, to measure the resolution actually obtained with this model of the experiment.

Some factors which can contribute to the loss of resolution are:

(1) energy lost by the alpha particle in escaping from the target,

(2) non-normal incidence of the alpha-particles on the detector surface,

(3) background noise generated by the target radioactivity.

A Po^{210} source, producing 5.3 Mev alpha particles, was used to investigate the loss of resolution due to the target radioactivity and the non-normal incidence of alpha particles on the detector surface. Curve A of Fig. 12 shows the 5.3 Mev alpha spectrum for essentially normal particle incidence and with no tritium target in the system. Curve B of Fig. 12 shows the spectrum obtained by moving the Po^{210} source to produce grazing incidence and adding the tritium target.

Figure 13 shows a typical pulse height spectrum due to 3.6 Mev deuterium-produced alpha particles (the Po^{210} source was included for calibration purposes). The spread in the spectrum is 600 Kev FWHM.

To test for possible background counts due to the target radioactivity, the Po^{210} source was removed and the ion beam shut off. At a potential of 80 kv no counts were observed during a period of about 10 minutes.

These results lead to the following conclusions:

(1) A tritiated target of 1 curie activity will not cause background counts in a silicon detector with a depletion depth of 90 microns.

(2) With this target and detector, 3.6 Mev alphas produced by the D-T reaction can be resolved to about 0.6 Mev.

(3) Most of the loss of resolution is due to target activity and non-normal incidence of particles on the detector surface.

Due to the complete isolation afforded by the infrared light-beam method of signal coupling, the 80 kv power supply had no observable effect on the measurement chain electronics, and hence, no effect on the resolution.

4.3 Deuterium Detector Efficiency

The efficiency of the instrument, in terms of counts per incident deuteron, was determined by measuring the counting rate produced by a known flux of deuterons incident on the outer grid of the instrument. The percentage of deuterium in the ion beam (Table I) was estimated by measuring beam current with and without the palladium leak on. All measurements of beam current were made after allowing the beam to reach a steady equilibrium.

Counting rate measurements were made for both atomic and molecular deuterium ions at energies of from 40 Kev to 80 Kev. The results for molecular deuterium have no direct significance, as molecular deuterium is not likely to exist in the solar wind, but were included to check the consistency of the measurements. As would be expected, the yield rates for D_2^+ ions are much lower than those for D^+ at the same accelerating voltage because each deuteron in the D_2^+ molecule has only half the total energy of the ion.

The results are tabulated in Table II. The efficiency in counts per D^+ and counts per D_2^+ is plotted as a function of accelerating potential in Fig. 14.

TABLE I

EFFICIENCY OF DEUTERIUM DETECTOR

Potential (kv)	Ion	Beam Current ($\times 10^{-10}$ A)	Counts Per 100 sec	Counts per Incident Ion ($\times 10^{-8}$)
80	D_2^+	5.40	811	0.233
70	"	4.95	353	0.111
60	"	4.20	128	0.0475
80	D^+	1.95	1248	1.33
70	"	1.93	719	0.775
60	"	1.92	380	0.412
50	"	1.90	163	0.179
40	"	1.87	50	0.056

TABLE II

DEUTERIUM CONTENT OF ION BEAM

Ion Energy (ev) (See Fig. 10)	310	580
Beam Current (Amps) (Palladium leak off)	10^{-12}	4.8×10^{-11}
Beam Current (Amps) (Palladium leak on)	6.2×10^{-10}	1.85×10^{-10}
Percent D^+ ions	0	75
Percent D_2^+ ions	100	0

These results were used to measure the relative abundance of deuterons in ordinary hydrogen gas. Figure 11 shows the ion source output with H_2 gas in the source. The ion beam contained deuterium in the forms HD^+ and D^+ (the amount of D_2^+ is negligibly small).

The relative abundance of deuterium in ordinary hydrogen was measured in the following way:

(1) The total ion source output was estimated from the graph of output current vs accelerating voltage (Fig. 11).

(2) Counting rates at 80 kv were measured at the HD^+ and D^+ peaks of the ion source output. No counts were observed except at these peaks.

(3) The previously measured efficiency of 1.3×10^{-8} counts per D^+ was used to compute the amount of D^+ in the beam.

(4) The measured efficiency of 0.23×10^{-8} counts per D_2^+ was corrected by a factor of 0.5 and used to compute the amount of HD^+ in the beam.

(5) The relative abundance of deuterium was taken to be the sum of the amounts of D^+ and HD^+ divided by the total output of the ion source. This procedure yielded a value of 2×10^{-4} for the relative abundance of deuterium. Since the known value is 1.4×10^{-4}, this result indicates that the measured efficiencies are accurate to within the experimental uncertainty.

Note that the efficiency measured for the deuterium detector is expressed in terms of counts per D^+ incident

was 1 curie, but its atomic ratio of tritium to zirconium and thickness were not known. It had been in storage for about one year before being used in this investigation.

4.4 Charge Spectrum Analyzer

It was important to evaluate the low-energy particle resolution which could be obtained with this detector and amplifier. This was done by observing the pulse height spectrum produced by an ion beam incident on the surface of the detector at a negative potential of 80 kv. The results are of limited value, however, because the ion source used for this test did not produce an appreciable number of multiply ionized particles.

Figure 15 shows a typical pulse height spectrum obtained at an accelerating potential of 80 kv. Tests were made at several values of ion beam charge-to-mass ratio, including those which correspond to singly-charged oxygen and carbon ions, but all pulse height spectra were essentially the same as that in Fig. 15.

The slope on the high-energy side of the pulse height spectrum indicates that there may have been a few doubly ionized particles present which could not be resolved into a peak by this instrument. It is apparent that the present resolution is not adequate. Increasing the bias voltage of the detector would have resulted in some improvements, but because most of the system noise was due to the preamplifier input stage, no attempt was made to optimize the detector bias voltage in this instrument.

The peak in the solar wind charge spectrum due to protons is expected to be much greater than the peak due to doubly ionized particles. If the system noise is assumed to be Gaussian, the normal distribution function can be used to estimate the FWHM resolution required to measure the number of doubly ionized particles to an accuracy of one percent in the presence of a large proton flux. Table III shows the values of equivalent FWHM noise calculated for several assumed ratios of doubly ionized particles to protons. The computations are given in Appendix B.

TABLE III

N^{++}/N^{+}	FWHM Noise in Kev (80 kv potential)	FWHM Noise in Kev (100 kv potential)
10^{-1}	32.9	40.7
10^{-2}	29.6	36.2
10^{-3}	27.3	33.8
10^{-4}	26.9	31.4

These values indicate that the 36 Kev FWHM noise of the present instrument is marginal, but a figure of 25 Kev FWHM should be entirely adequate. It would be desirable to achieve a lower figure than this, however, to allow for the gradual degradation of detector performance due to radiation damage (D2).

A total system resolution of 25 Kev FWHM would be difficult to achieve with a transistor preamplifier, although it may be possible (F2). However, much lower noise figures (3 to 5 Kev FWHM) have been quoted for preamplifiers using field-effect transistors in the input stage (F2, B1). An amplifier of this type is presently being developed for use in the charge spectrum analyzer.

Appendix A: The High Voltage Power Supply

A1. Field Configuration

Due to large potential gradients associated with small radii of curvature, great care must be taken in high voltage design to eliminate sharp edges, points or rough surfaces. In vacuum, gradients on the order of 10^8 volts per meter can cause cold field emission from negative electrode surfaces. Field emission is thought, in many cases, to be the first step in the chain of events which leads to complete voltage breakdown of the vacuum gap (M1).

These problems were encountered repeatedly in the construction of a negative 100 kv supply for an earlier experiment (see Fig. 3). The aluminum discs (corona shields) in the present power supply (Fig. 4) are designed to shield the parts of the structure which could otherwise generate large voltage gradients. In particular, the metal film electrodes on each of the capacitors are shielded by mounting the capacitor in a shallow circular depression in the corona shield surface. This provides a slight overhang which places the edge of the capacitor in a region of essentially constant potential. The points where diode leads are connected are also shielded by being recessed into the surface of the corona shield.

A2. Construction

The barium titanate capacitors used for this power supply were unencapsulated disc-shaped units 1 inch in diameter and 5/16 inch thick. The two series-connected capacitor stacks each consisted of nine corona shields and eight capacitors cemented together with conducting epoxy (Alaco Conducting 20-20) to form a column. The 16 kv diodes were then connected between the appropriate corona shields in each column by press fitting the wire leads into holes. Each lead was cemented in place with a drop of conducting epoxy, care being taken to prevent the excess epoxy from protruding above the smooth surface of the corona shield. At this point the two capacitor columns were held together by 16 diodes, 8 on each side. To relieve the mechanical stress on the diode leads, the structure was then cemented to a rigid base (Fig. 4).

The completed structure was first tested in insulating oil where it reached its rated voltage of 80 kv. When tested in vacuum, however, each stage would support only 3 to 4 kv, although the capacitors were each rated at 10 kv. This confirmed the result of an earlier test in which individual unencapsulated capacitor units tested in vacuum would break down along the surface at about 4 kv while those tested in oil or silicone rubber would easily stand rated voltage.

The entire capacitor-diode structure of the power supply was encapsulated in RTV-11 silicone rubber potting

compound. The dipping method of encapsulation was chosen to minimize the quantity of rubber on the supply which later would have to be cured. To prevent the possibility of voids in the rubber, the complete dipping operation was carried out in vacuum.

Two dippings were required to produce a sufficiently thick coat of rubber. Each coat was cured for several days at 50°C. After the second curing period, the rubber was allowed to outgas in vacuum for several more days before the power supply was tested.

When tested, it achieved its rated voltage of 80 kv without difficulty, showing none of the characteristic symptoms associated with vacuum breakdown.

Table IV gives a breakdown, by weight, of the components in the capacitor-diode structure.

TABLE IV

Component	Unit Weight (grams)	Number	Total Weight (grams)
Capacitor	19.2	16	307.2
Diode	4.1	16	49.6
Corona shield	15.9	18	286.2
Potting compound, Base, Epoxy, etc.			446.0
TOTAL			1089

A3. Problems

The most serious difficulty encountered with this supply was the low mechanical strength of the barium titanate capacitors. After the supply had been assembled, but before it had been encapsulated, three of the ceramic capacitors were chipped or broken and required replacement. The supply had been cleaned several times in an ultrasonic bath and it was suspected that this had caused at least two of the capacitor failures by exciting resonant vibrations in the columns which shattered the capacitors.

The axial wire leads on the 16 kv diodes were another source of trouble. These wire leads were not shielded from high potential gradients where they entered the diode. The large electrical stresses existing around these leads were made evident by the fact that the silicone rubber on three of the leads was punctured when the power supply experienced heavy arcing along its outer surface during the early testing of the field focusing structure. Fortunately these punctures did not effect the operation of the supply.

A4. Recommendations

This power supply was built only to allow the laboratory testing of the deuterium detector and charge spectrum analyzer. It fulfilled this purpose very satisfactorily and also provided some valuable experience in the field

of vacuum high-voltage engineering. Nevertheless, it is not intended to represent the answer to the high-voltage problem for this experiment.

A suitable power supply design for space application must be evaluated in terms of:

(1) weight

(2) volume

(3) total power and efficiency

(4) reliability

(5) temperature sensitivity

(6) mechanical strength

(7) regulation

(8) ripple.

Because of the essentially no-load operating condition, the efficiency and regulation are less important than the other factors. The ripple must be evaluated because it will tend to reduce the charge spectrum resolution.

In designing the present supply, the value of 10 kv per stage was chosen to be compatible with a given driver transformer. In future designs, however, the first step should be to study various possible driver transformers in terms of power consumption, weight, and volume as functions of maximum output voltage. This should determine an optimum value of voltage-per-stage, and therefore the total number of stages required.

The use of mica capacitors to replace the ceramic capacitors has been considered briefly and appears

attractive for future designs. Several manufacturers custom-design capacitors of pressed mica for special applications. It seems that an integrated capacitor column should be possible.

The diodes used in future designs should be ordered with special anti-corona shields to alleviate the problems due to the wire leads. It is also recommended that these diodes be overrated in voltage as this helps to protect them against damage due to surges.

The silicone rubber, RTV-11, seems to be a satisfactory insulating material for vacuum high-voltage application. Repeated arcing along its surface did not damage it in any way and it appeared to stop outgassing appreciably after an initial conditioning period. Unlike the LTV series of silicone compounds used in earlier attempts, RTV-11 adhered well to smooth surfaces.

Appendix B: Electronics

B1. Amplifier

The object of the "charge sensitive" preamplifier is to make the input capacitance of the preamplifier much greater than the detector capacitance. Variations in detector capacitance due to ambient conditions or changes in bias voltage then do not affect the output signal amplitude. The output voltage of a charge sensitive amplifier is given by

$$V_o = \frac{Q_i}{C_f}$$

where V_o is the output signal amplitude, Q_i is the charge deposited on the input terminal, and C_f is the feedback capacitor. (This expression assumes infinite frequency response.) This approximation holds if the open loop voltage gain, A_v is negative and meets the condition

$$|A_v| \gg 1.$$

The input capacitance of the amplifier is given by

$$C_i = C_{io} + (A_v + 1)C_f$$

where C_{io} is the input capacitance of the amplifier with feedback loop open. In the common emitter configuration C_{io} is dominated by the "Miller effect," which increases the collector-base capacitance, C_{bc}, by a factor equal to the voltage gain of the transistor. The cascode connection used in the input stage of this preamplifier

eliminates the Miller effect by holding the collector of the input transistor at an essentially constant voltage (E1). In this way C_{io} is held to a value approximately equal to C_{bc}, which is much less than $A_v C_f$, so

$$C_i \lesssim A_v C_f$$

The noise performance of the preamplifier is controlled to a large extent by its frequency response. The purpose of the capacitors C_1 and C_2 (Fig. 7) is to shape the frequency response of the system to produce a maximum signal-to-noise ratio. The optimum performance for most transistors is obtained at equal integrating and differentiating time constants of 1 microsecond (E1,F2). This places the center of the amplifier passband at about 170 kc.

With this frequency response, the preamplifier produces an exponentially rising and falling pulse whose peak amplitude is

$$V_p \lesssim .37 \frac{Q_i}{C_f}$$

While it improves the gain stability, the large input capacitance of the preamplifier decreases the signal-to-noise ratio because it does not reduce the noise voltage to the same degree that it does the signal voltage. For this reason, the preamplifier used for low energy particle detection in the charge spectrum analyzer was designed to have an input capacitance approximately

equal to the detector capacitance. Figure 19 shows that the input capacitance of the preamplifier, with a 2pf feedback capacitor, is about 50 pf. Since the detector capacitance is 80 pf at 4 volts bias, this amplifier cannot be considered "charge sensitive" in the true sense of the word.

B2. Calibration and Noise Measurement

The equivalent noise of the system is defined as the energy of a particle which would produce a voltage signal of peak amplitude exactly equal to the system RMS noise voltage. From the normal distribution function the FWHM (full-width-at-half-maximum) noise is found to be 2.35 times the equivalent noise. The FWHM figure is generally used in the literature.

In the depletion region of a silicon detector, one electron-hole pair is created for each 2.35 ev of energy lost by a charged particle passing through the region. This figure is relatively independent of the species of ionizing particle or its total energy over a wide range of energies (01). If the depletion region is thick enough to completely stop the particle, the signal is directly proportional to the total particle energy over a wide range of non-relativistic velocities.

The standard method for calibrating solid state particle detector systems is to deposit on the input terminal an amount of charge equivalent to a specified

particle energy. For a 100 kv particle the equivalent charge is $(10^5)(2.35^{-1})(1.6 \times 10^{-19}) = 4.6 \times 10^{-15}$ coul. The equivalent charge is deposited in a time interval short compared with the amplifier rise time by connecting a square wave generator or mercury pulser to the amplifier input through a small capacitor. In this case a 1 mv square wave, produced by a voltage divider, and a 5 pf capacitor provided a calibrate signal of about 5×10^{-15} coul. — roughly equivalent to 108 kev.

To measure the noise due to the amplifier alone, the detector is replaced by an equivalent capacitor and a pulse height spectrum is taken of the system output with the calibrate signal as an input. If the pulse height analyzer has first been calibrated in kev per channel, the FWHM noise can be taken directly from the spectrum (Fig. 23). The detector can then be replaced and the process repeated to measure the total system noise. Since the detector and amplifier noise sources are independent, the total system noise should be given by

$$N_S^2 = N_D^2 + N_A^2$$

where N_S is the total system source and N_D and N_A the detector and amplifier noises.

Figure 18 is a plot of amplifier noise versus external capacitance. Figure 17 is a plot of the detector capacitance versus bias voltage. It can be

seen from these two plots that a detector bias of 4 volts is hardly an optimum value. It was chosen, however, to eliminate the need for another battery inside the high potential shell.

Figure 23 shows a typical pulse height spectrum obtained with calibrate signals equivalent to 100 kev and 200 kev. The FWHM noise is seen to be 36 kev. This includes the detector noise. The infrared signal transmission system did not contribute appreciably to the total system noise.

B3. Resolution for Charge Spectrum Analysis

Due to the expected predominance of protons in the solar wind, the peak in the charge spectrum corresponding to singly charged particles should be large compared to the peaks for multiply charged particles. The normal distribution function can be used to estimate the resolution required to resolve the doubly-charged peak out of the "tail" of the singly charged peak.

The singly charged peak can be represented by

$$n_1 = \frac{N_1}{\sqrt{2\pi}\,\sigma_1}\, e^{-\frac{1}{2}\left(\frac{E-E_o}{\sigma_1}\right)^2}$$

where n_1 = number of particles per unit energy

N_1 = total number of singly charged particles

σ_1 = standard deviation in kev of peak due to singly charged particles

E = energy in kev

E_o = average energy in kev (accelerating potential)

In the same way the doubly charged peak is represented by

$$n_2 = \frac{N_2}{\sqrt{2\pi}\,\sigma_2} \quad e^{-\frac{1}{2}\left(\frac{E-2E_o}{\sigma_2}\right)^2}$$

The standard deviations, σ_1 and σ_2, are due to a combination of system noise, ripple on the power supply, and the random initial energies of the ions entering through the sampling grid. To count 99 percent of the doubly ionized particles, the lower discriminator level for the second peak should be at about $(2E_o - 2.6\,\sigma_2)$.

The condition imposed now is that the number of counts above this discriminator level due to singly charged ions be less than one percent of the total number of doubly charged ions. Assuming σ_1 and σ_2 are equal, this is,

$$\int_{(2E_o-2.6\sigma)}^{\infty} \frac{N_1}{\sqrt{2\pi}\,\sigma} \; e^{-\frac{1}{2}\left(\frac{E-E_o}{\sigma}\right)^2} \, dE < .01N_2$$

In terms of the tabulated normal distribution function this is

$$\int_{x_o}^{\infty} \varphi(x) \quad < \quad .01\,\frac{N_2}{N_1}$$

where $x_o = \left(\frac{E_o}{\sigma} - 2.6\right)$

Now for an assumed value of N_2/N_1, x_o can be found from the tables. Then the FWHM noise required for a given accelerating potential can by found from

$$\text{FWHM} = \frac{2.35\,E_o}{x_o+2.6}$$

Table III gives the calculated values of allowable FWHM noise in Kev for several values of N_2/N_1 for accelerating potentials of 80 kv and 100 kv.

B4. Infrared Signal Coupling

As mentioned in Chapters III and IV, a photomultiplier tube was used in this model of the experiment to serve as a receiver for the infrared signal transmission system. Since it would be desirable to replace the phototube with a smaller, less fragile device, the possibility of using a solid state light sensor was investigated. The LSX-400 (Texas Instruments Corp.), whose spectral response curve most nearly matches the GaAs diode emission spectrum, had a rise time which was much too long to make it suitable.

The LSX-400 was replaced by a 25 mm^2 solid state particle detector of the same type as used for the charge spectrum analyzer. The detector responded well to the 0.9 micron wavelength radiation emitted by GaAs and showed a rise time of about 4 microseconds. Figure 21 shows the detector DC current as a function of detector bias voltage and GaAs diode current. This curve was plotted using a flexible fiberoptics light pipe to guide the light beam to the sensitive surface of the detector.

With a voltage amplifier on the infrared detector, this system worked as well as the photomultiplier tube.

It was not used in testing the deuterium detector and charge spectrum analyzer, however, because the flexible light pipe would not support the 80 kv accelerating potential.

These results are preliminary at best, but are mentioned here because they seem to warrant further investigation.

BIBLIOGRAPHY

(B1) T.V.Blalock, "A Low-Noise Charge-Sensitive Preamplifier with a Field-Effect Transistor in the Input Stage" IEEE Trans. NS-11, 365 (1964).

(B2) H.C.Bourne, "A Study of the Theory of Voltage Breakdown in High Vacuum," M.I.T. Sc.D. Thesis, Course IV, 1952.

(B3) E.M.Burbidge, G.R.Burbidge, W.A.Fowler, and F.Hoyle, "Synthesis of Elements in Stars," Rev. Mod. Phys. 29, 547 (1957).

(B4) D.A.Bryant, T.L.Cline, U.D.Deasi, and F.B.McDonald, "Studies of Solar Protons with Explorers XII and XIV" NASA GSFC Preprint X-611-64-217 (1964).

(D1) A.S.Denholm, "The Space Environment as a Dielectric," Dielectrics in Space Symposium, Westinghouse Research Lab., June 25-26, 1964.

(D2) G.Dearnaley, "Radation Damage by Charge Particles in Silicon Junction Detectors," IEEE Trans. NS-10, 106 (1963).

(E1) T.L.Emmer, "Low Noise Transistor Amplifiers for Solid State Detectors," IRE Trans. NS-8, 140, (1961).

(F1) W.A.Fowler, J.L.Greenstein, and F.Hoyle, "Nucelosynthesis during the Early History of the Solar System," Geophys. J., 6, 148 (1961).

(F2) S.S.Freidland, H.S.Katzensen, and F.P.Zimba, "Advances in Semiconductor Detectors for Charged Particle Space Spectrometry," IEEE Trans. NS-10, 190 (1963).

(G1) L.Goldberg, O.C.Mohler, and E.A.Muller, "The Profile of Hα During the Limb Flare of February 10, 1956," Astrophys. J. 127, 302 (1958).

(G2) J.L.Greenstein, "A Search for He^3 in the Sun," Astrophys. J., 113, 531 (1951).

(G3) J.L.Greenstein and R.S.Richardson, "Lithium and the Internal Circulation of the Sun," Astrophys. J., 119, 536 (1951).

(G4) J.L.Greenstein and E.Tandeberg-Hannsen, Astrophys. J., 119, 113 (1954).

(G5) E.M.Gunnersen and G.James, "On the Efficiency of the Reaction H(d,n) He^4 in Titanium Tritide Bombarded with Deuterons," Nuc. Inst. and Meth., 8, 173 (1960).

(H1) L.Heller, "Theories of Element Synthesis and the Abundance of Deuterium," Astrophys. J., 126, 341 (1957).

(K1) T.D.Kinman, "An Attempt to Detect Deuterium in the Solar Atmosphere," Monthly Notices of Royal Astronomical Society, 116, 77 (1956).

(K2) M.J.Kofoid, "Effect of Metal-Dielectric Junction Phenomena on High-Voltage Breakdown over Insulators in Vacuum," AIEE Trans. III, 79, 999, (1960).

(M1) D.R.Mott, "Measurement of Particle Currents in High-Voltage Breakdown," M.I.T. B.S. Thesis, 1959, Course VI.

(M2) P.Morrison, private communication to F. Scherb of M.I.T. Laboratory of Nuclear Science.

(O1) Oak Ridge Technical Enterprises Corp., "Surface Barrier Detector Instruction Manual."

(S1) E.E.Salpeter, "Nuclear Reactions in the Stars I. Proton-Proton Chain," Phys. Rev. 88, 547 (1952).

(S2) E.E.Salpeter, Nuclear Reactions in Stars II. Protons on Light Nuclei," Phys. Rev. 97, 1237 (1955).

(S3) H.J.Smith and E.V.P.Smith, "Solar Flares," The Macmillan Co. 1963.

(S4) C.W.Snyder and M.Neugebauer, "Interplanetary Solar Wind Measurements by Marina II," J.P.L. Report, Cont. No. NASA-7-100.

LIST OF FIGURES

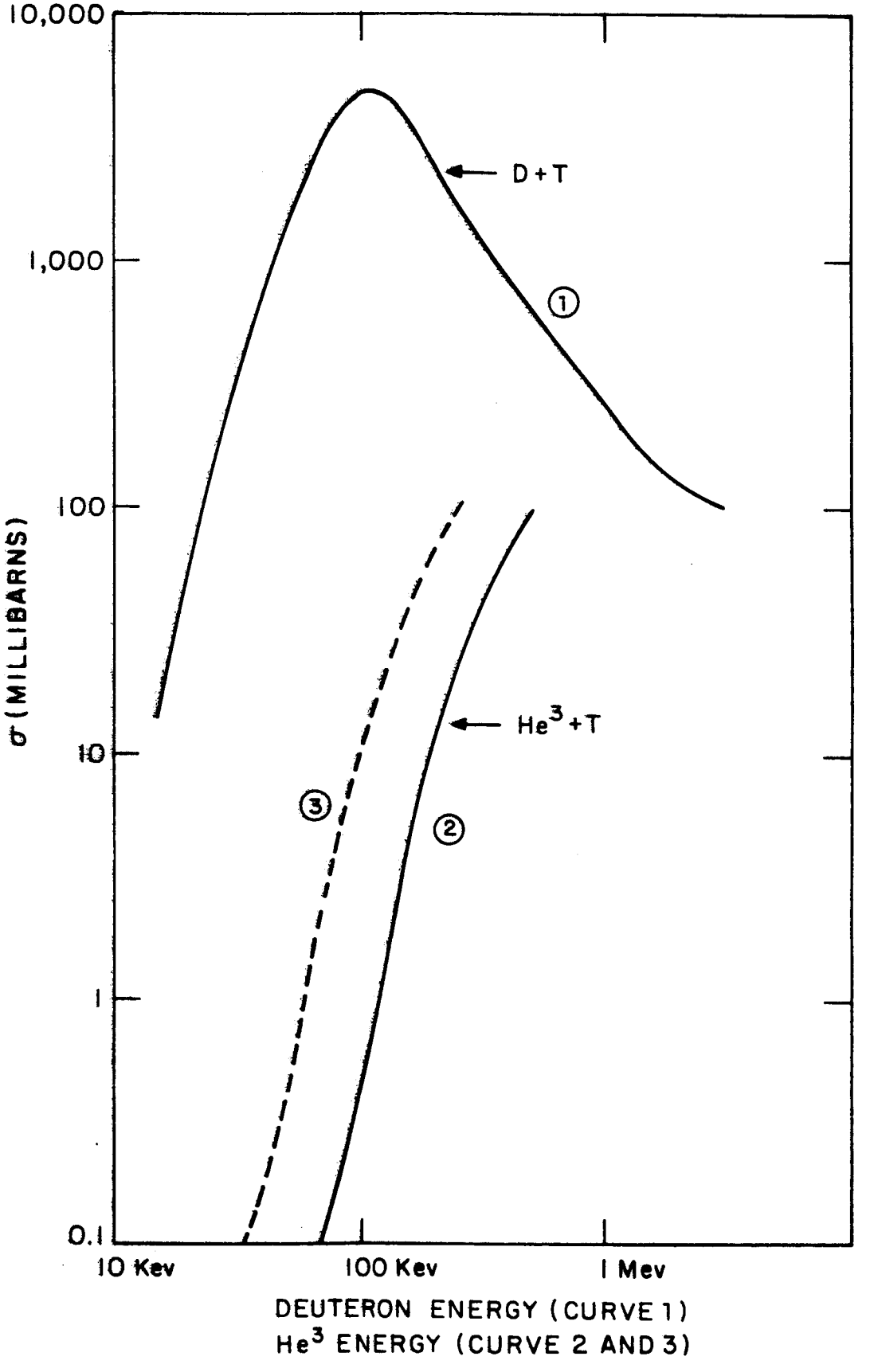
10,000
1,000
100
10
1
0.1
σ (MILLIBARNS)
D+T
①
He³+T
②
③
10 Kev
100 Kev
1 Mev
DEUTERON ENERGY (CURVE 1)
He³ ENERGY (CURVE 2 AND 3)

FIGURE 1

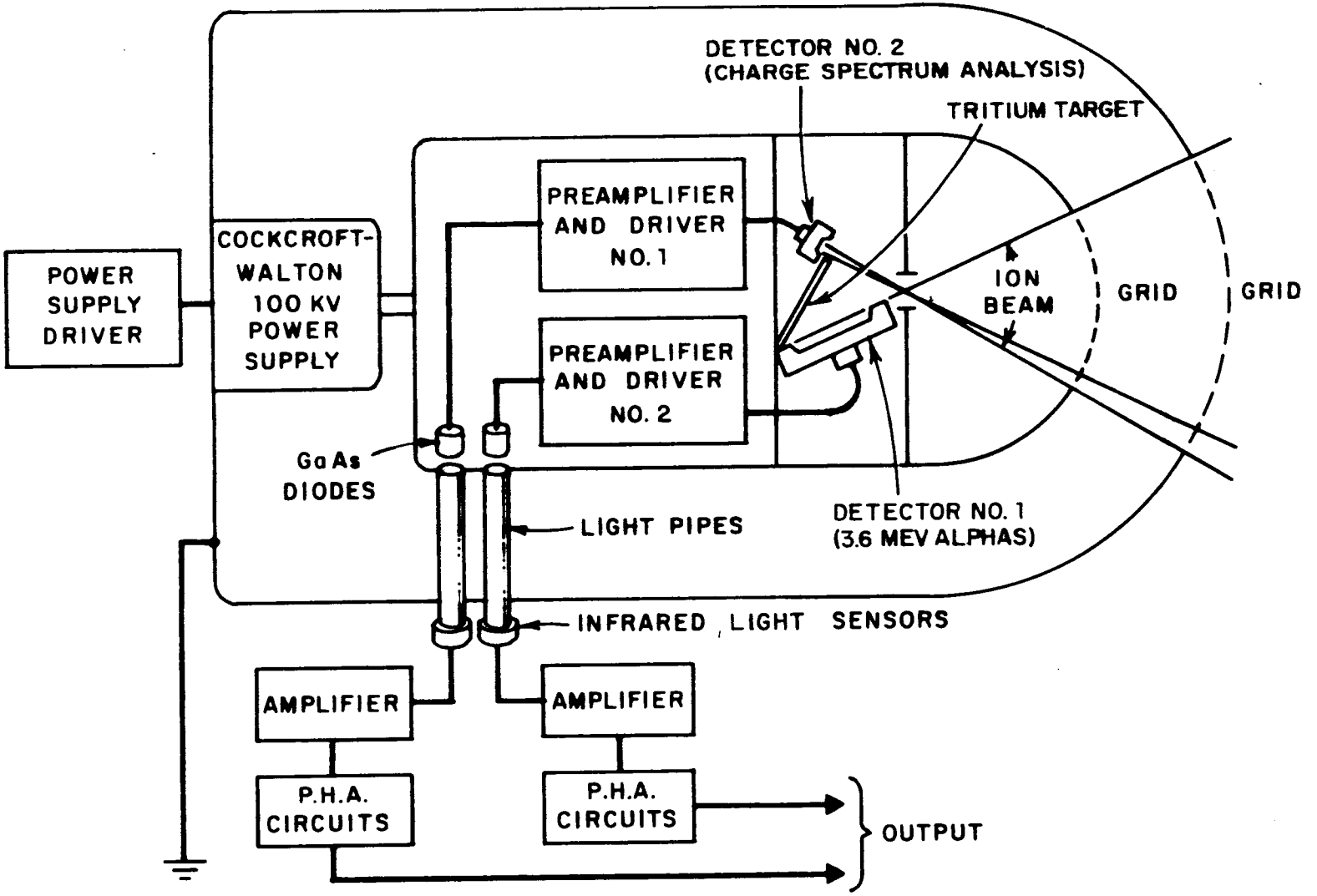
DETECTOR NO. 2
(CHARGE SPECTRUM ANALYSIS)
TRITIUM TARGET
PREAMPLIFIER AND DRIVER NO. 1
PREAMPLIFIER AND DRIVER NO. 2
POWER SUPPLY DRIVER
COCKCROFT-WALTON 100 KV POWER SUPPLY
ION BEAM
GRID
GRID
GaAs DIODES
LIGHT PIPES
DETECTOR NO. 1
(3.6 MEV ALPHAS)
INFRARED LIGHT SENSORS
AMPLIFIER
AMPLIFIER
P.H.A. CIRCUITS
P.H.A. CIRCUITS
OUTPUT

FIGURE 2

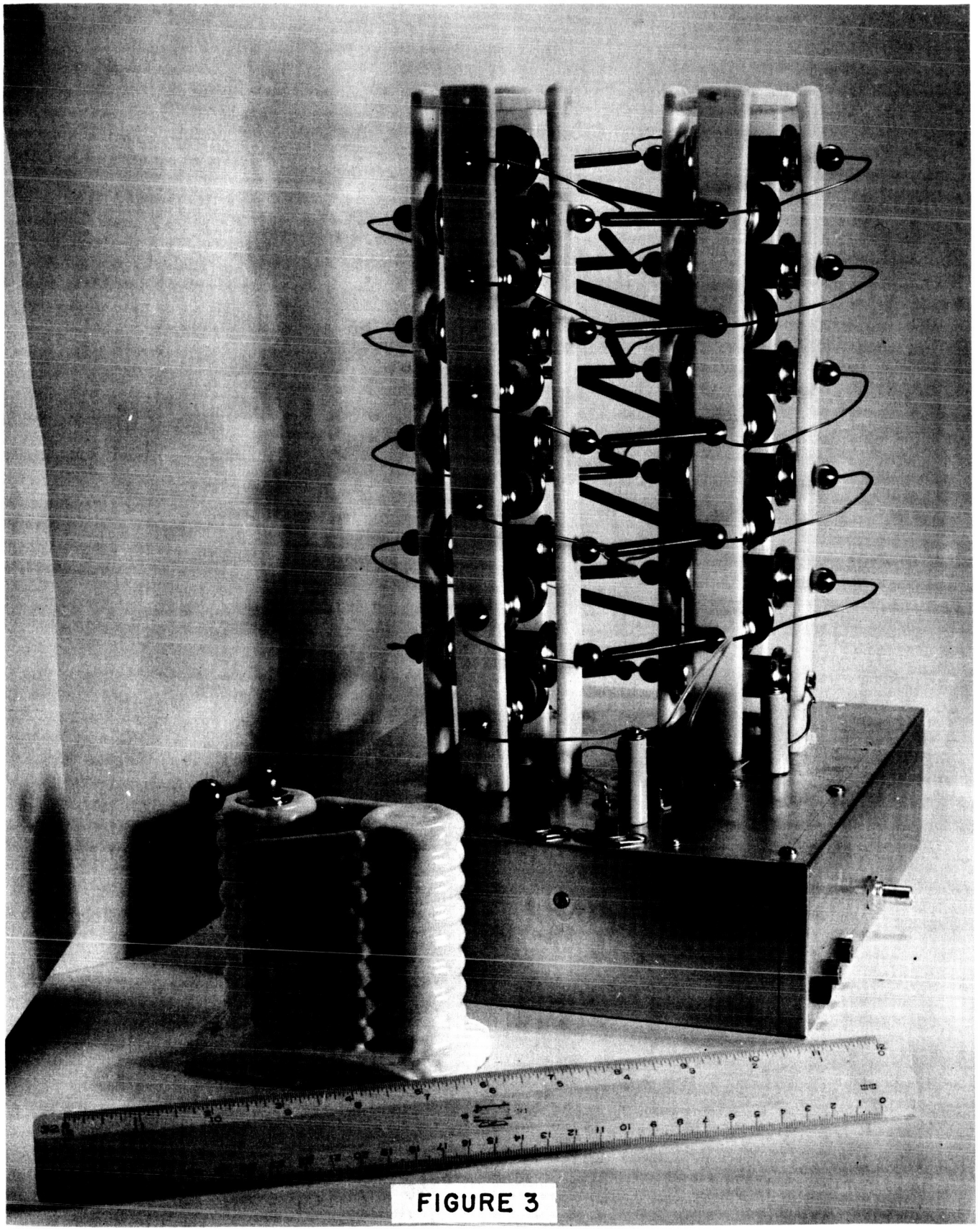

FIGURE 3

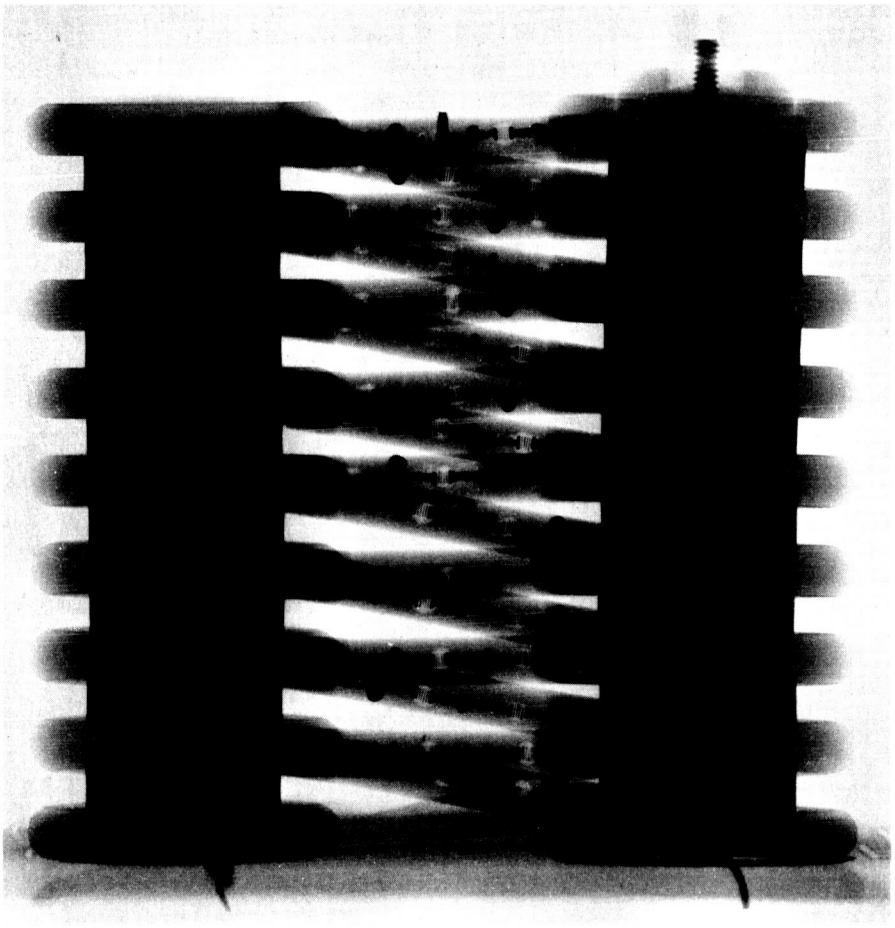

FIGURE 4

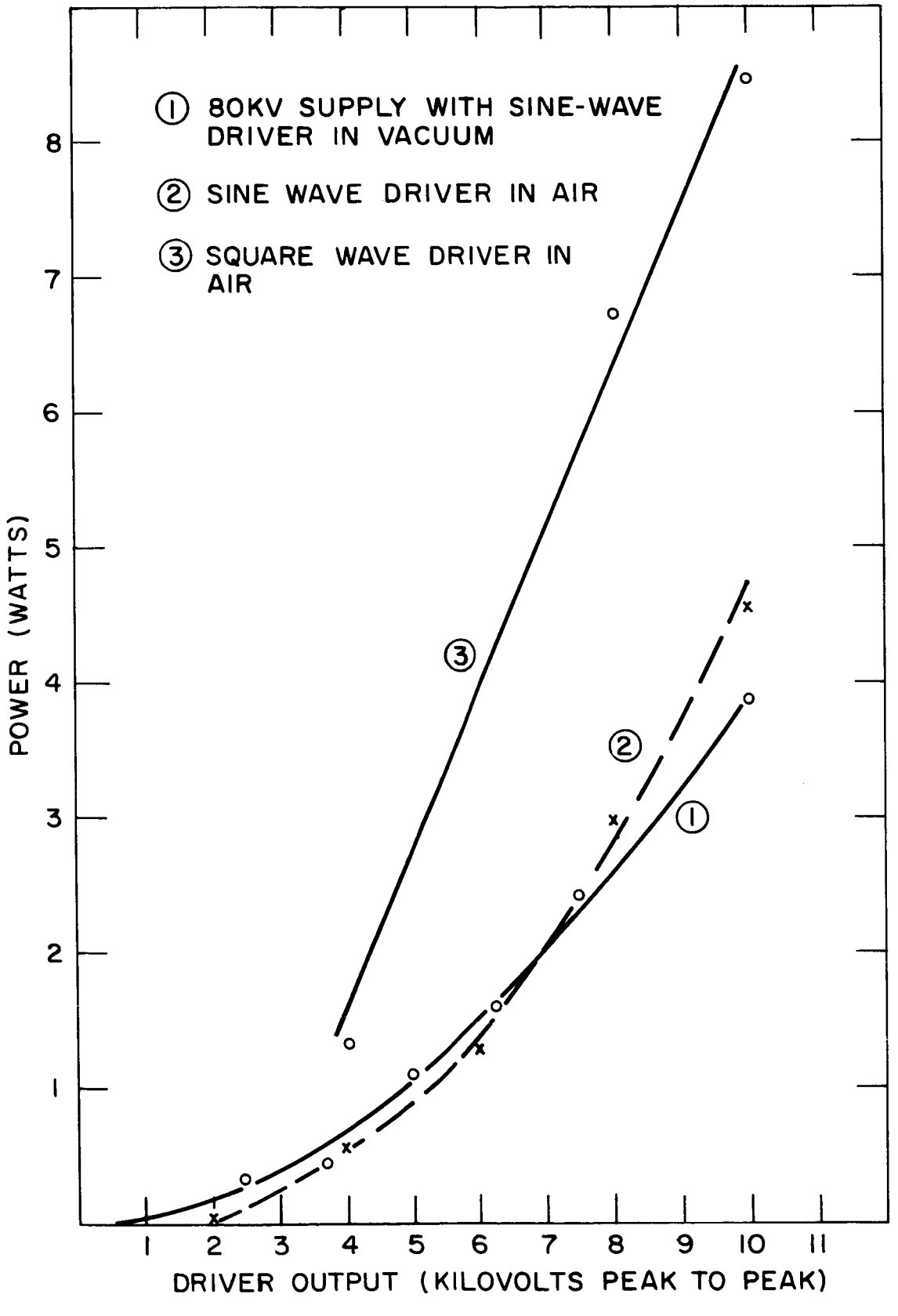
① 80KV SUPPLY WITH SINE-WAVE DRIVER IN VACUUM
② SINE WAVE DRIVER IN AIR
③ SQUARE WAVE DRIVER IN AIR
POWER (WATTS)
1
2
3
4
5
6
7
8
1 2 3 4 5 6 7 8 9 10 11
DRIVER OUTPUT (KILOVOLTS PEAK TO PEAK)

FIGURE 5

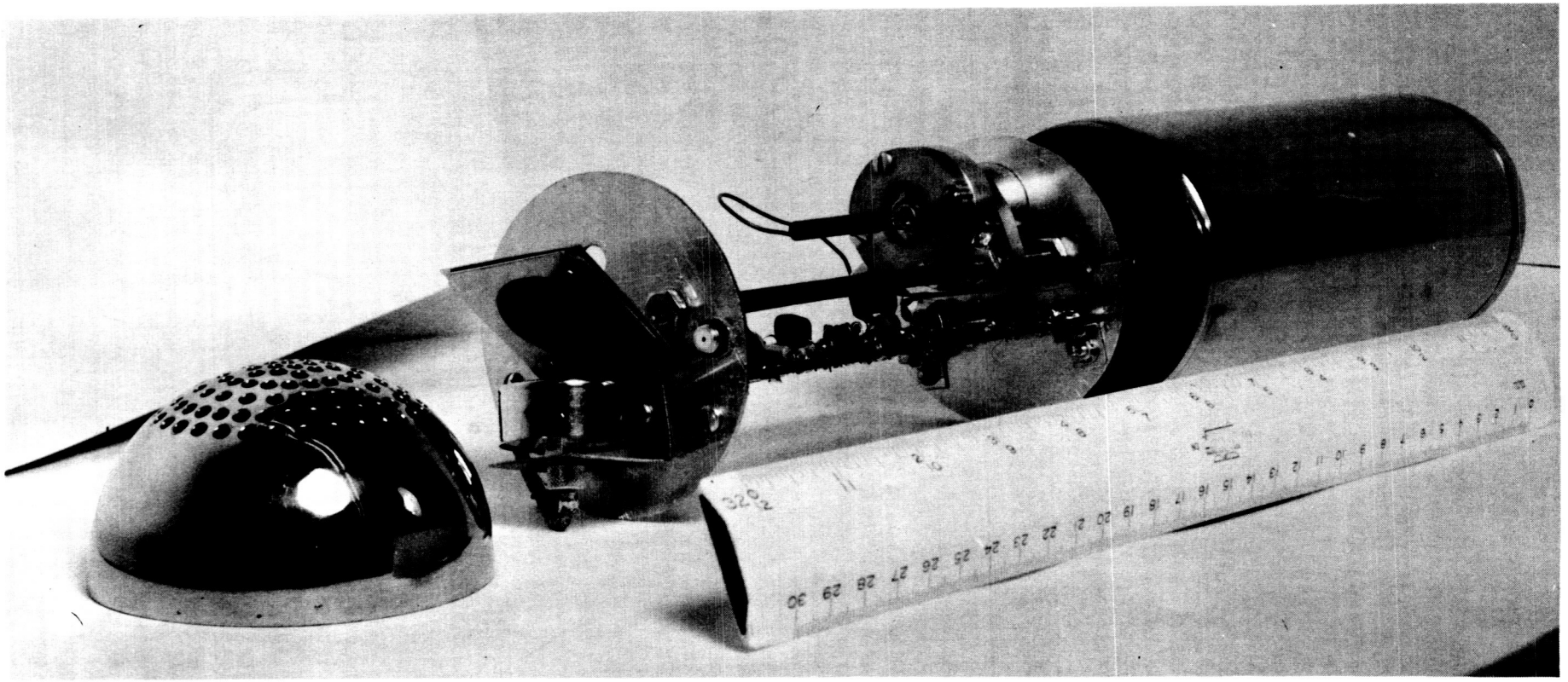

FIGURE 6

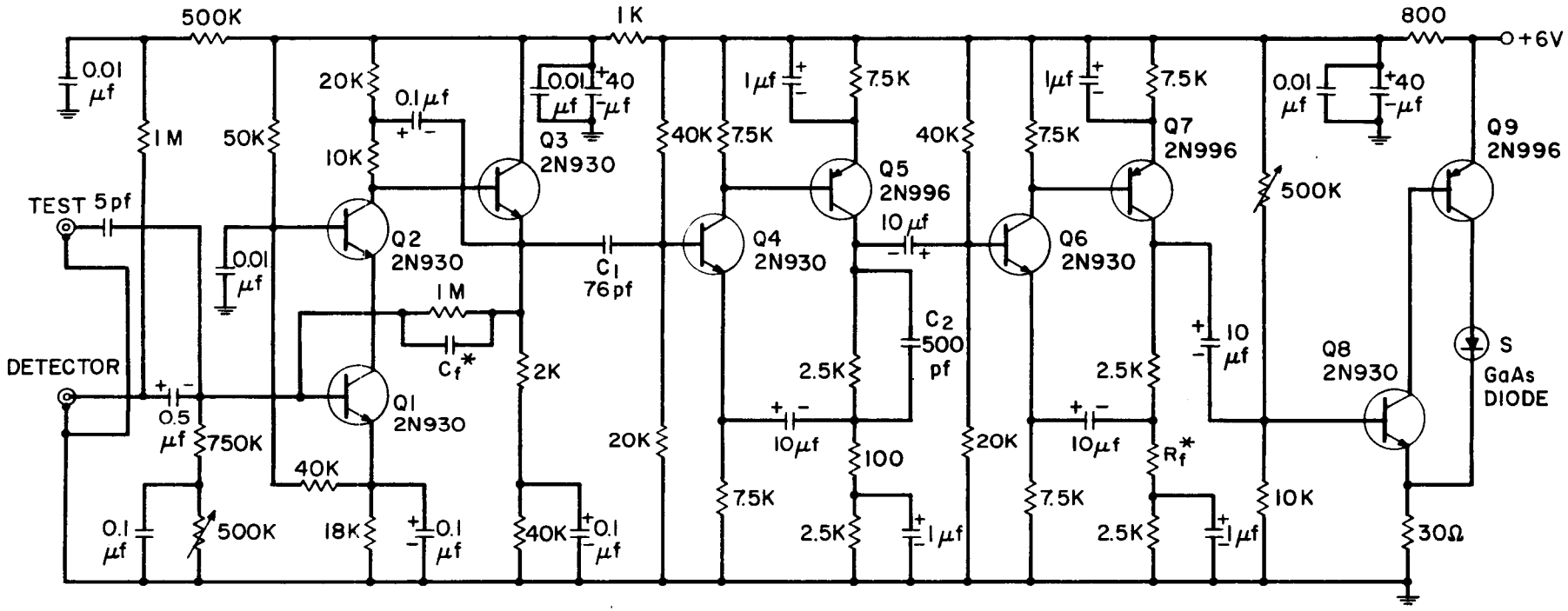

	C_f	R_f
DEUTERIUM DETECTOR	10pf	100
CHARGE SPECTRUM ANALYZER	2pf	25

FIGURE 7

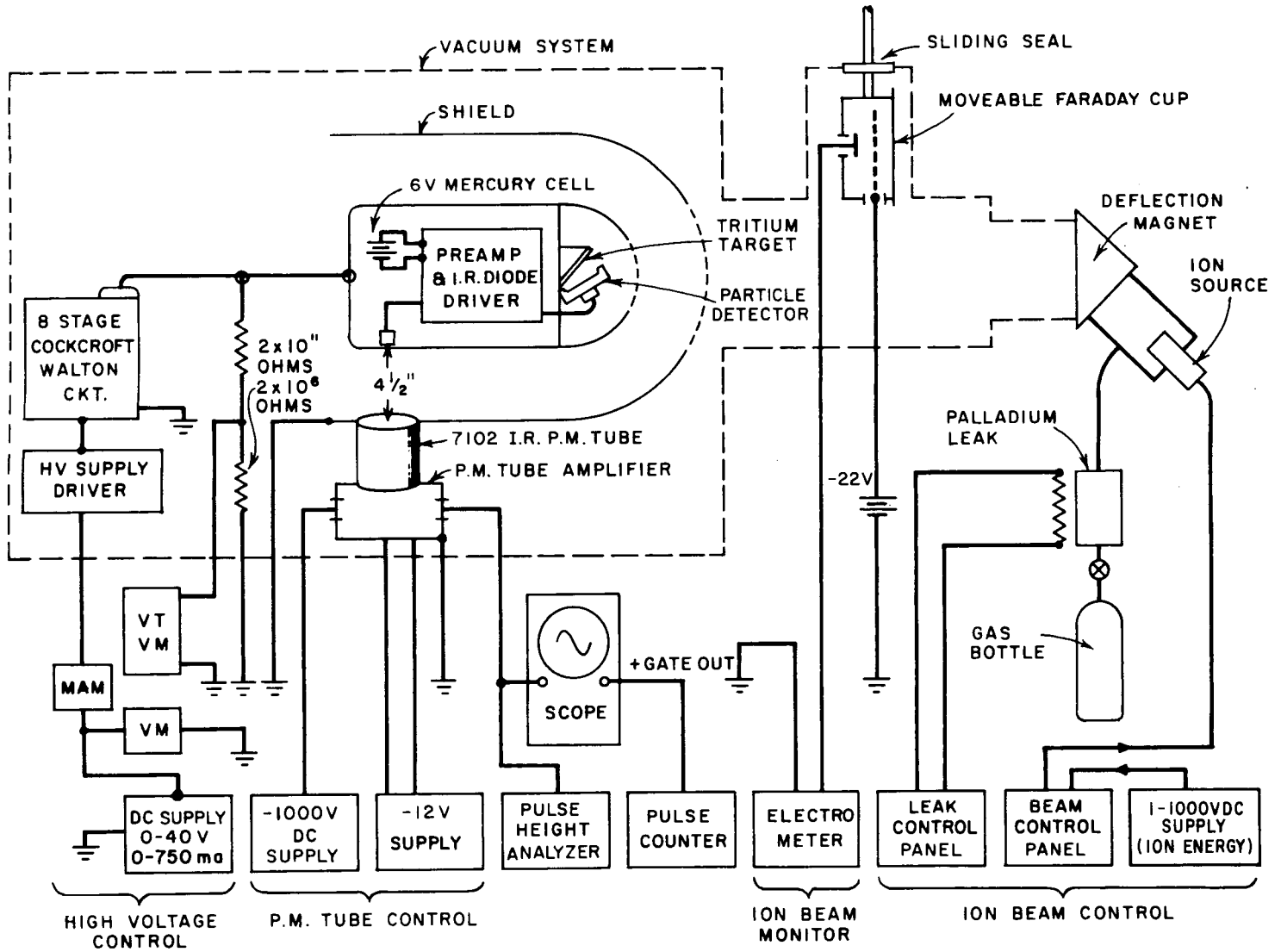
VACUUM SYSTEM
SHIELD
6V MERCURY CELL
PREAMP & I.R. DIODE DRIVER
TRITIUM TARGET
PARTICLE DETECTOR
SLIDING SEAL
MOVEABLE FARADAY CUP
DEFLECTION MAGNET
ION SOURCE
8 STAGE COCKCROFT WALTON CKT.
2x10" OHMS
2x10⁶ OHMS
4½"
7102 I.R. P.M. TUBE
P.M. TUBE AMPLIFIER
HV SUPPLY DRIVER
-22V
PALLADIUM LEAK
GAS BOTTLE
VT VM
MAM
VM
SCOPE
+GATE OUT
DC SUPPLY 0-40V 0-750 ma
-1000V DC SUPPLY
-12V SUPPLY
PULSE HEIGHT ANALYZER
PULSE COUNTER
ELECTRO METER
LEAK CONTROL PANEL
BEAM CONTROL PANEL
1-1000VDC SUPPLY (ION ENERGY)
HIGH VOLTAGE CONTROL
P.M. TUBE CONTROL
ION BEAM MONITOR
ION BEAM CONTROL

FIGURE 8

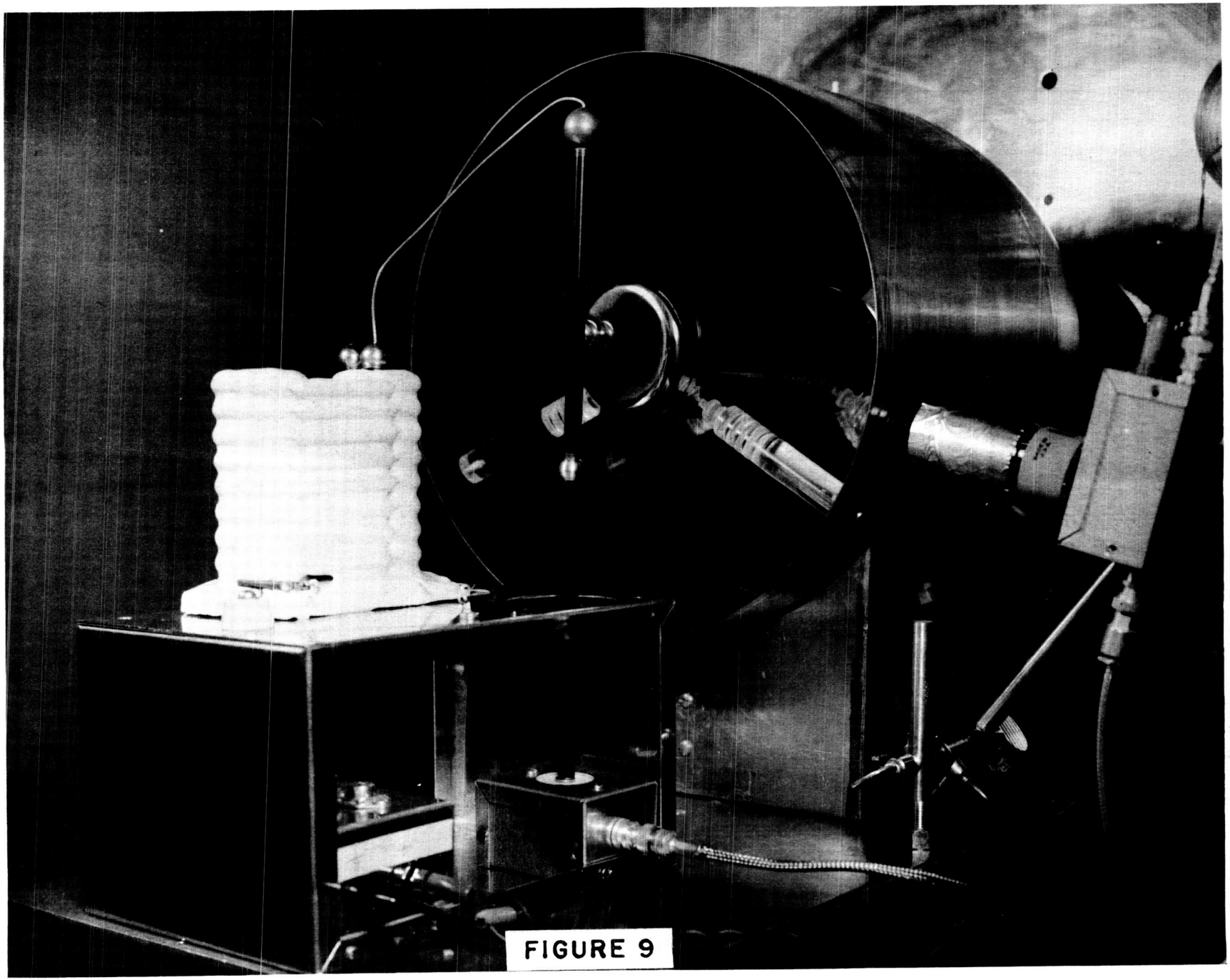

FIGURE 9

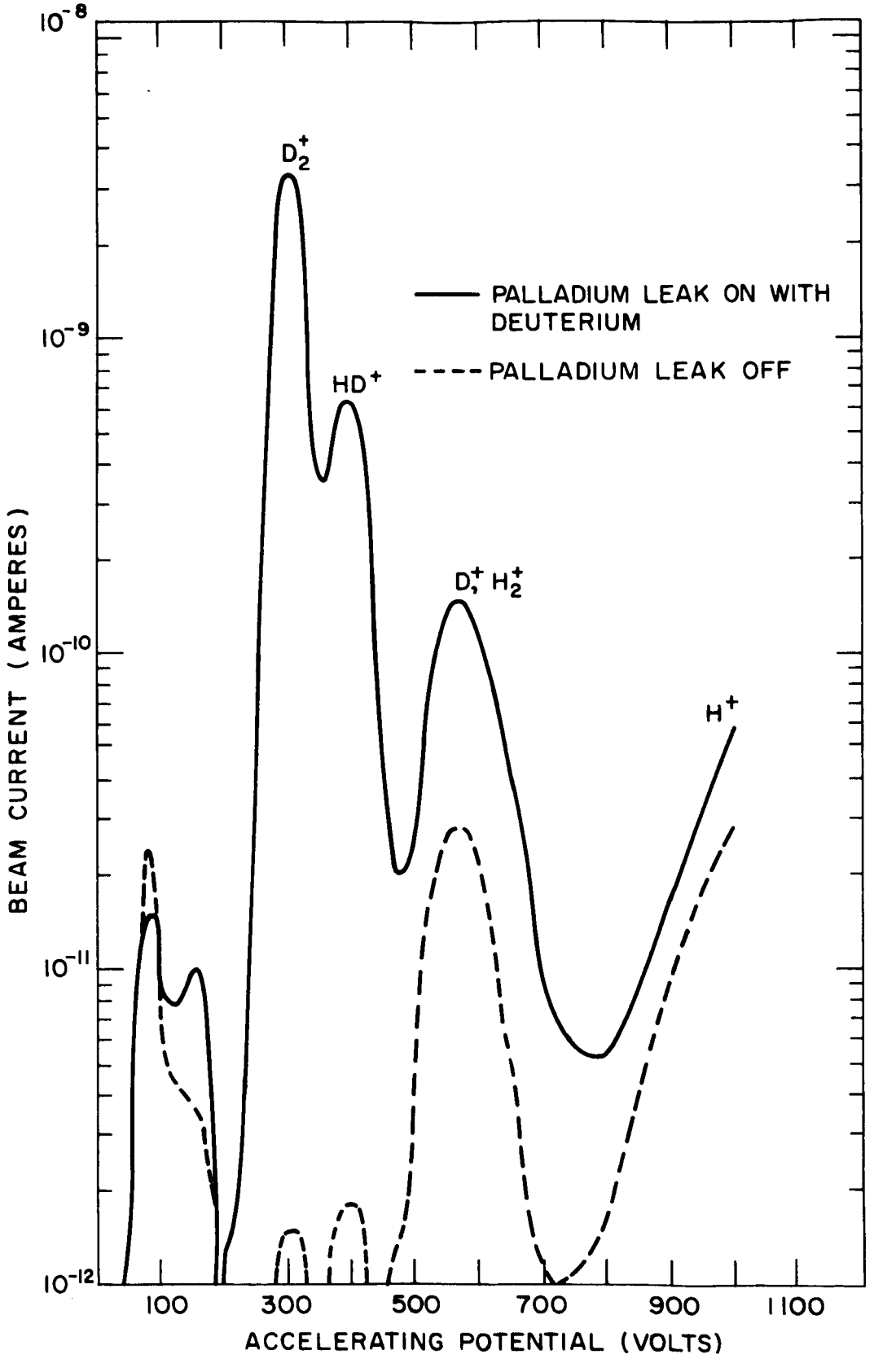
10^{-8}
10^{-9}
10^{-10}
10^{-11}
10^{-12}
BEAM CURRENT (AMPERES)
D_2^+
HD^+
D_2^+ H_2^+
H^+
PALLADIUM LEAK ON WITH DEUTERIUM
PALLADIUM LEAK OFF
100
300
500
700
900
1100
ACCELERATING POTENTIAL (VOLTS)

FIGURE 10

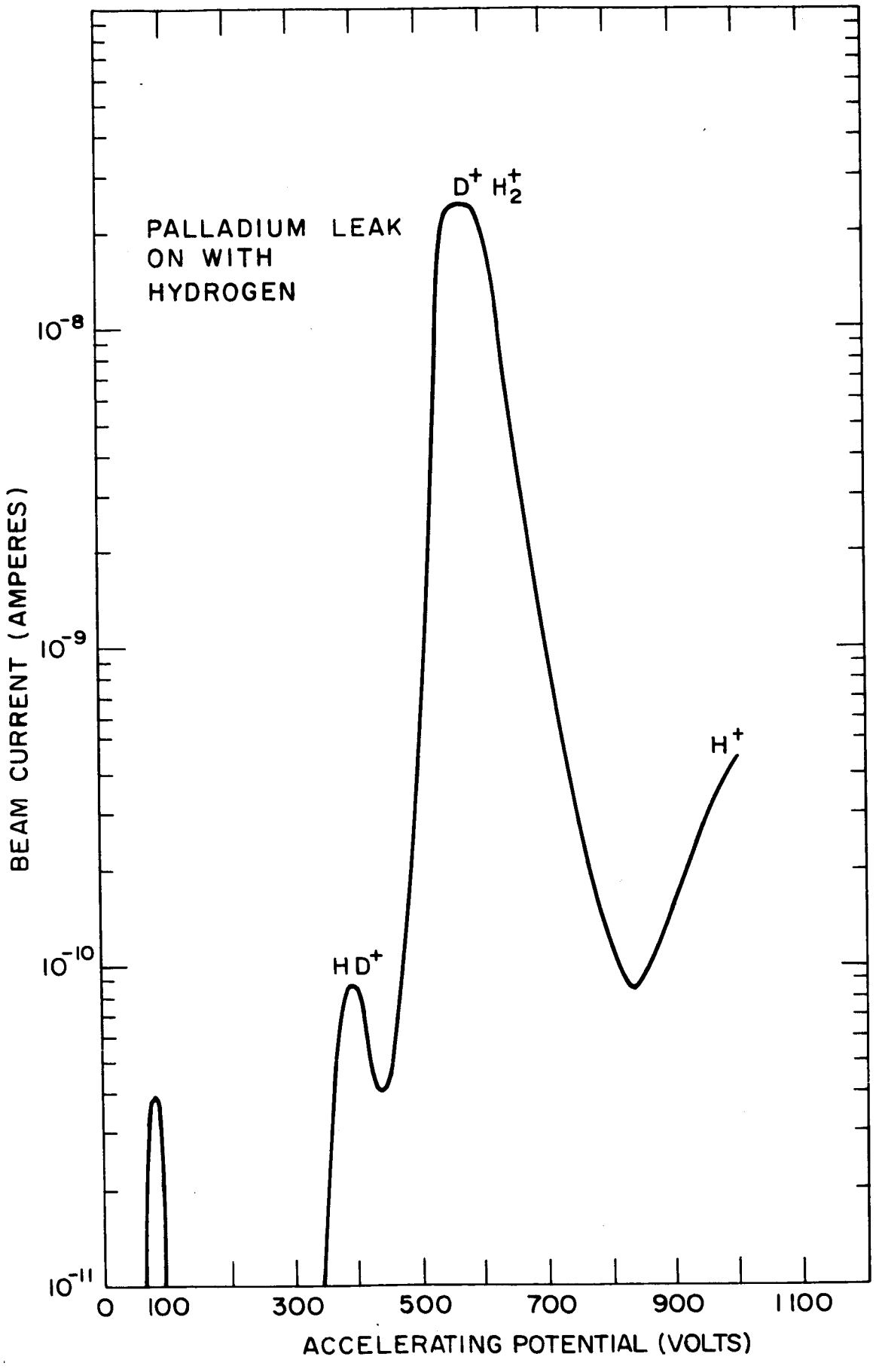
PALLADIUM LEAK
ON WITH
HYDROGEN
D+ H2+
H+
HD+
BEAM CURRENT (AMPERES)
10-8
10-9
10-10
10-11
0
100
300
500
700
900
1100
ACCELERATING POTENTIAL (VOLTS)

FIGURE 11

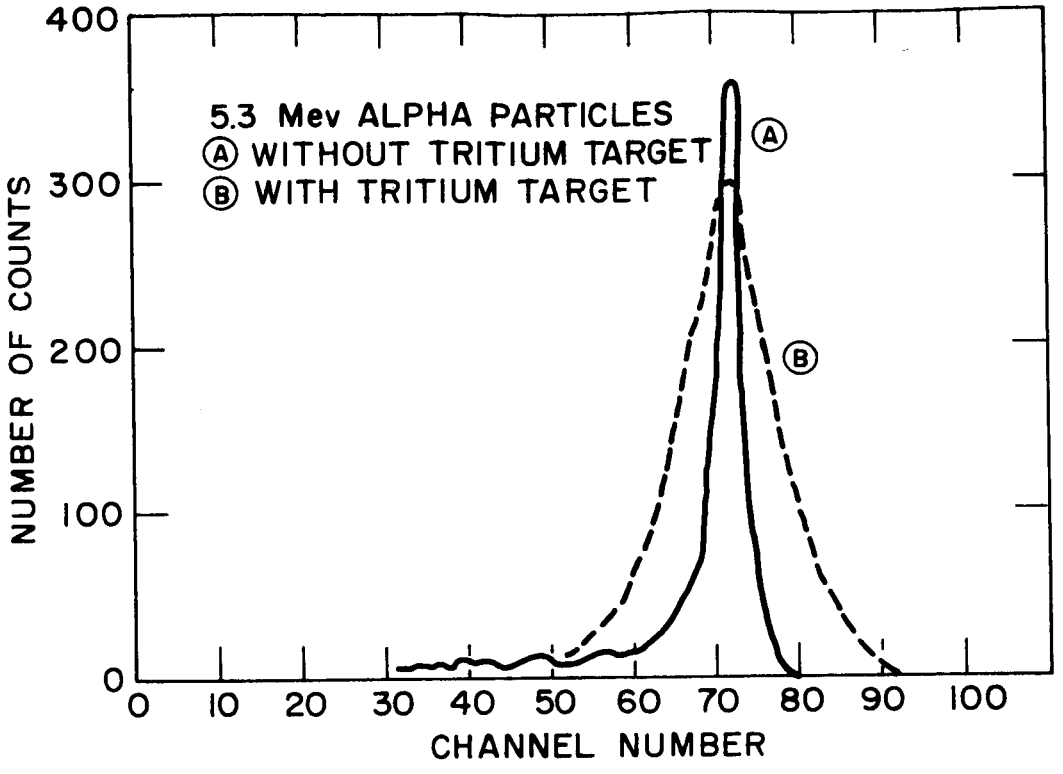

FIGURE 12

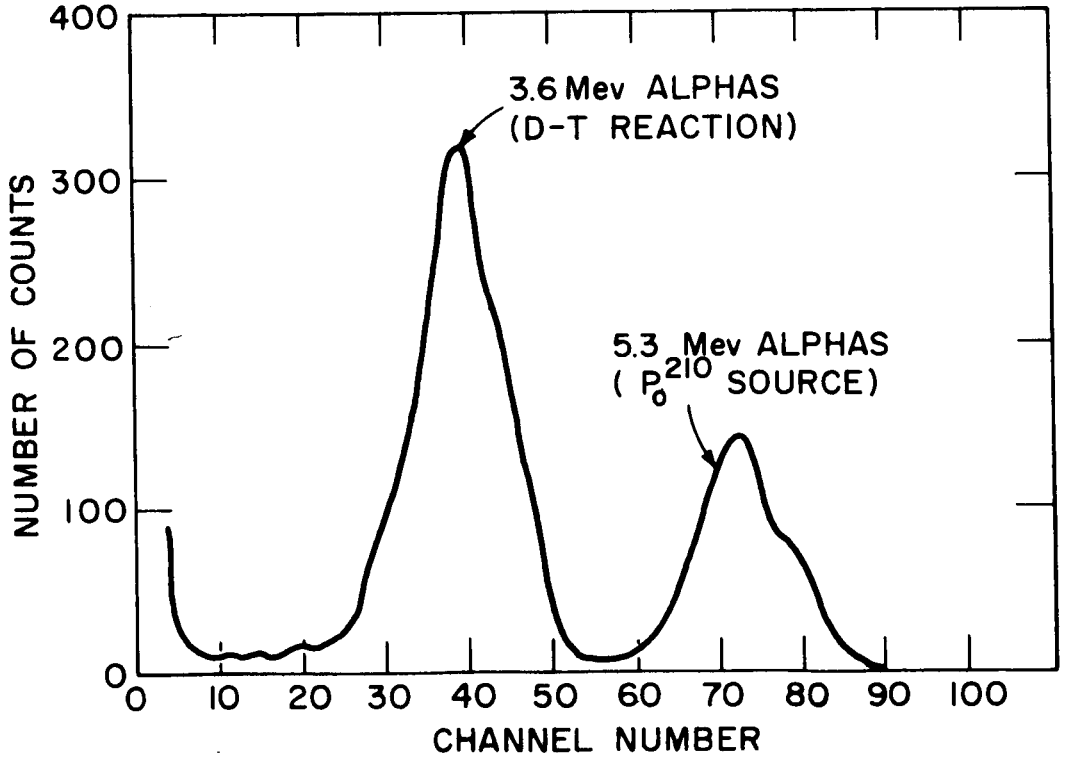

FIGURE 13

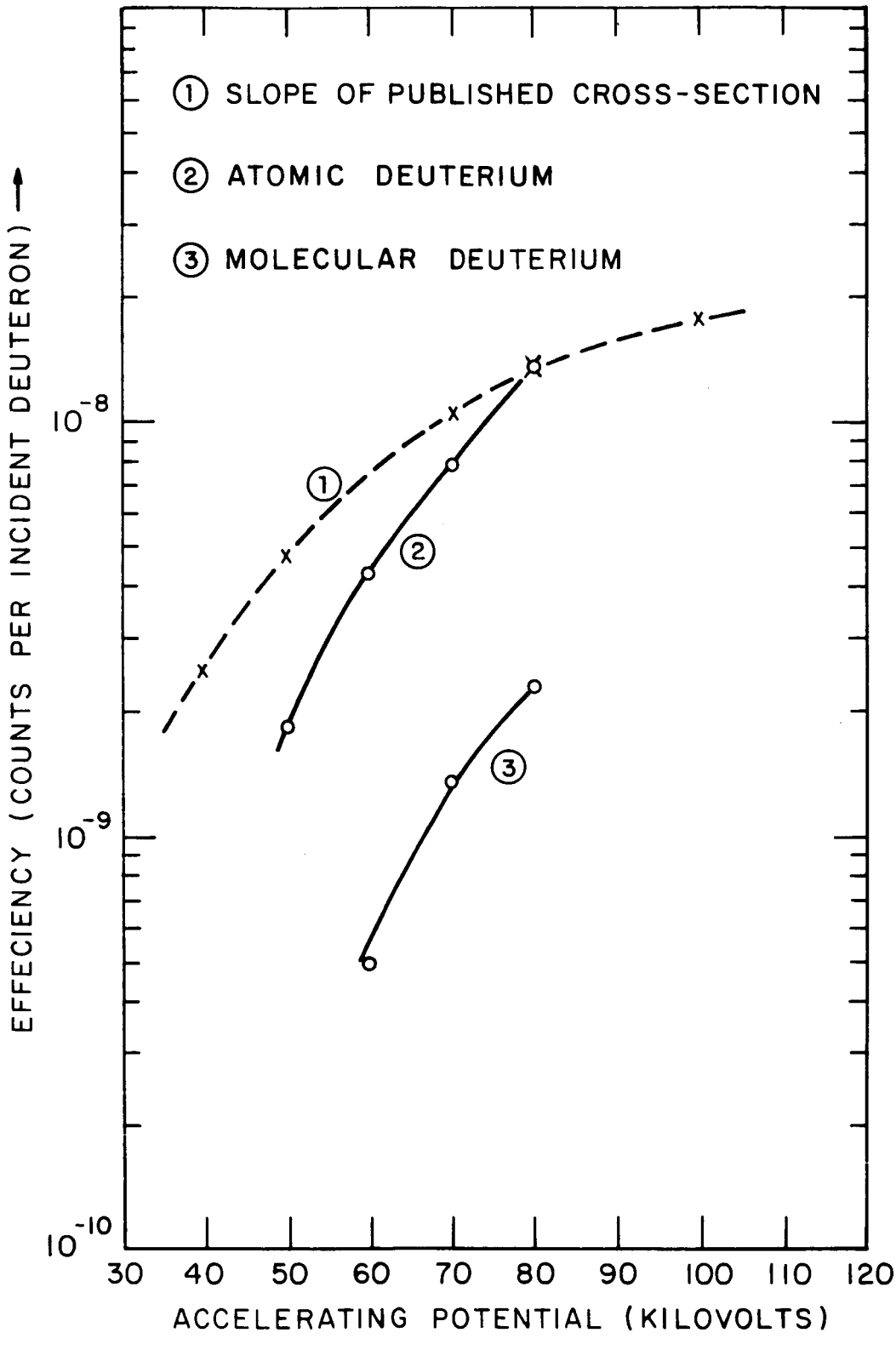
① SLOPE OF PUBLISHED CROSS-SECTION
② ATOMIC DEUTERIUM
③ MOLECULAR DEUTERIUM
EFFECIENCY (COUNTS PER INCIDENT DEUTERON)
10^{-8}
10^{-9}
10^{-10}
30 40 50 60 70 80 90 100 110 120
ACCELERATING POTENTIAL (KILOVOLTS)

FIGURE 14

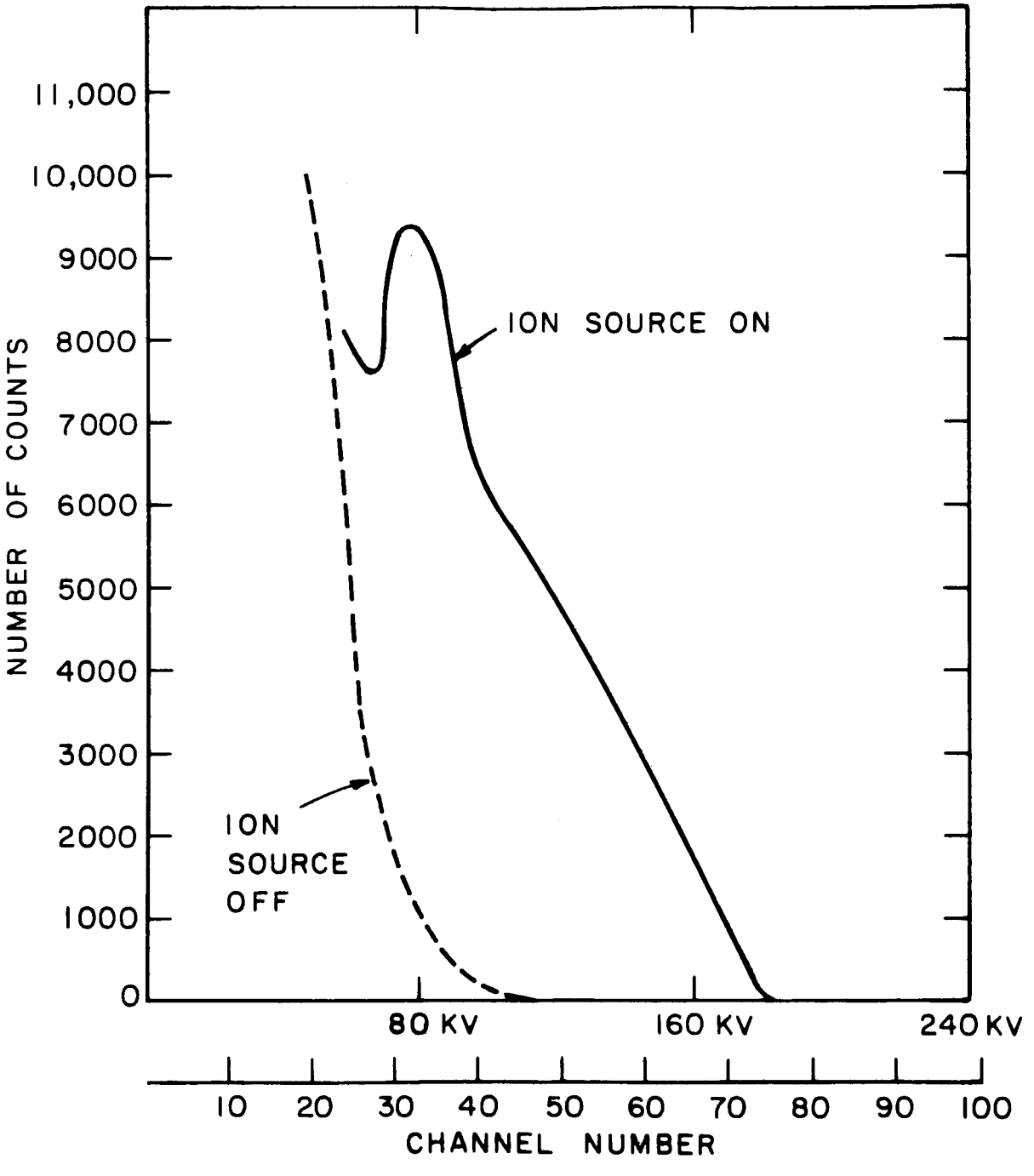
11,000
10,000
9000
8000
7000
6000
5000
4000
3000
2000
1000
0
NUMBER OF COUNTS
ION SOURCE ON
ION
SOURCE
OFF
80 KV
160 KV
240 KV
10
20
30
40
50
60
70
80
90
100
CHANNEL NUMBER

FIGURE 15

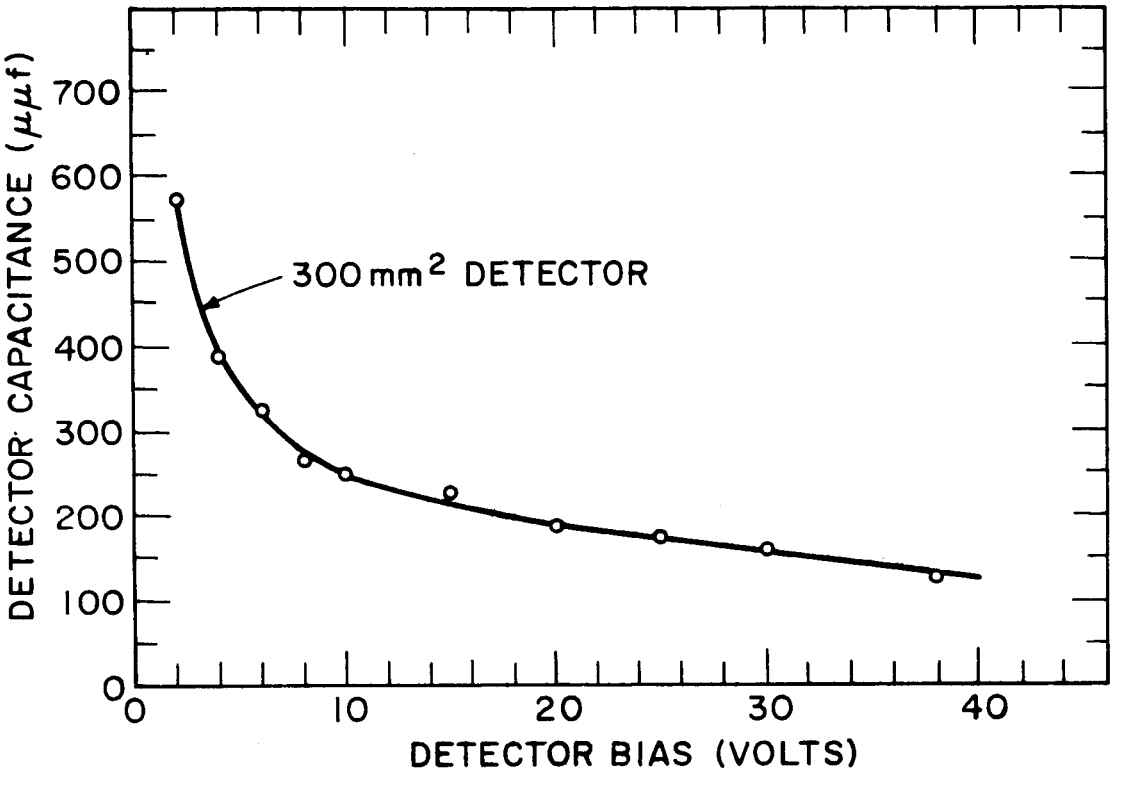

FIGURE 16

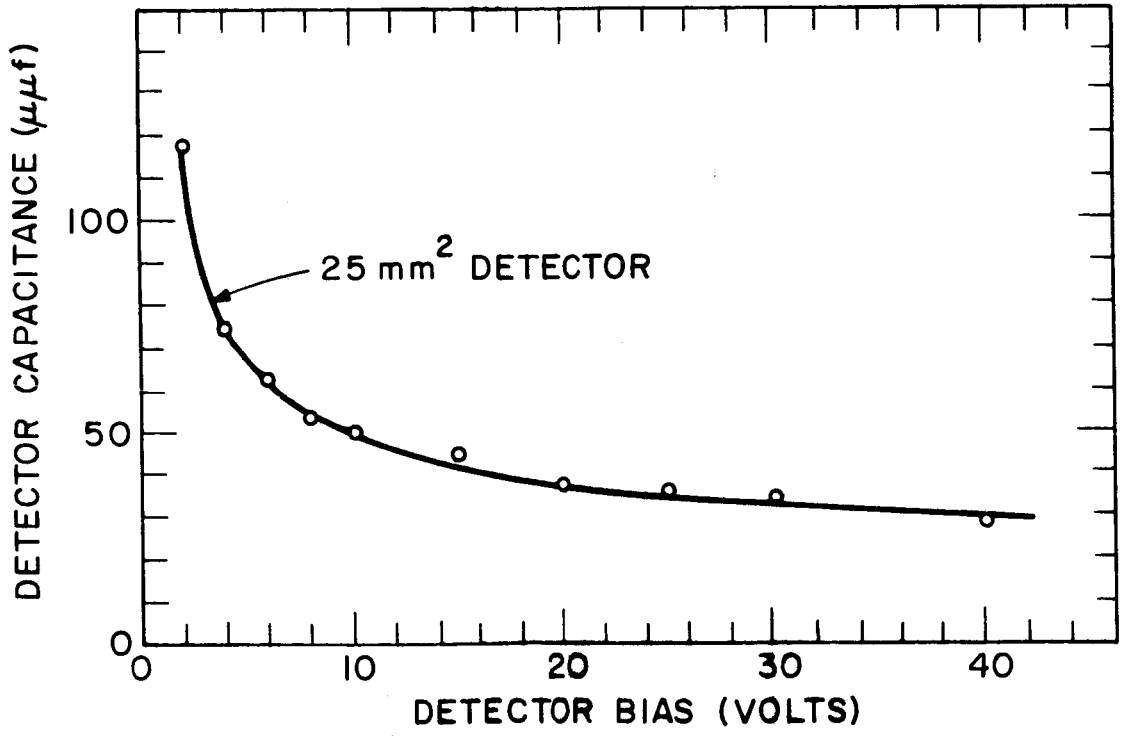

FIGURE 17

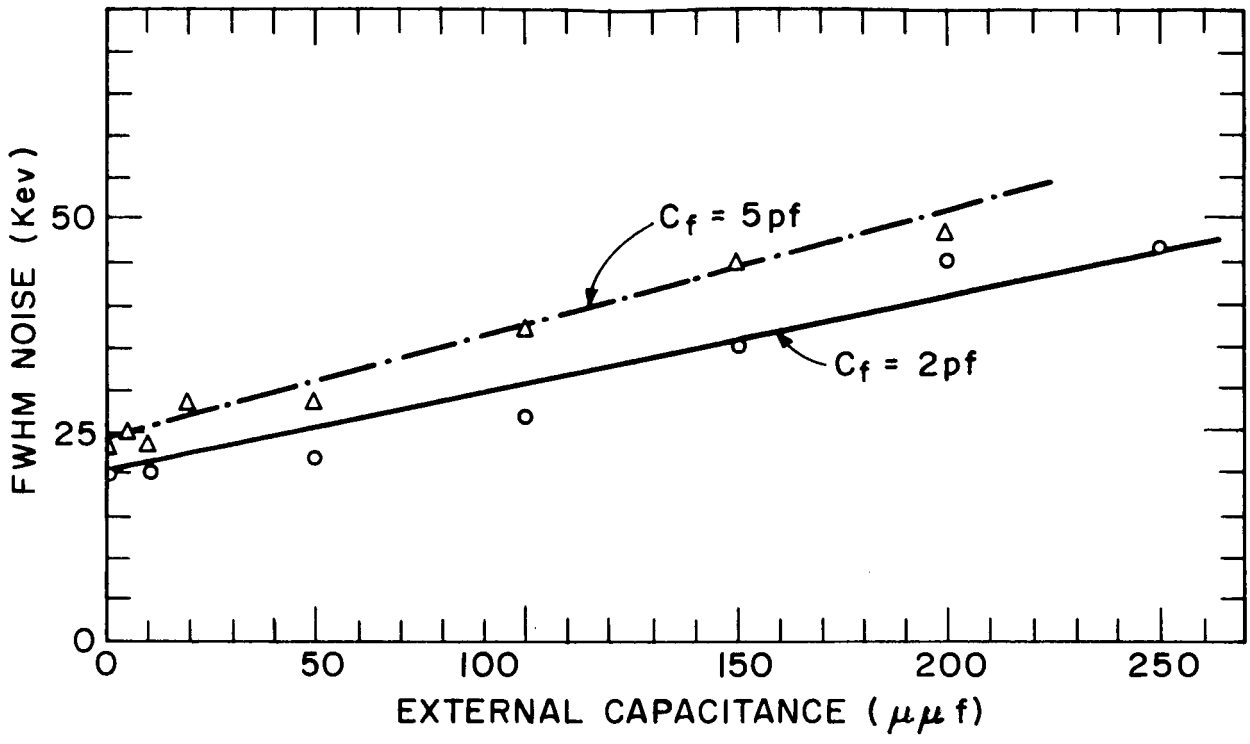

FIGURE 18

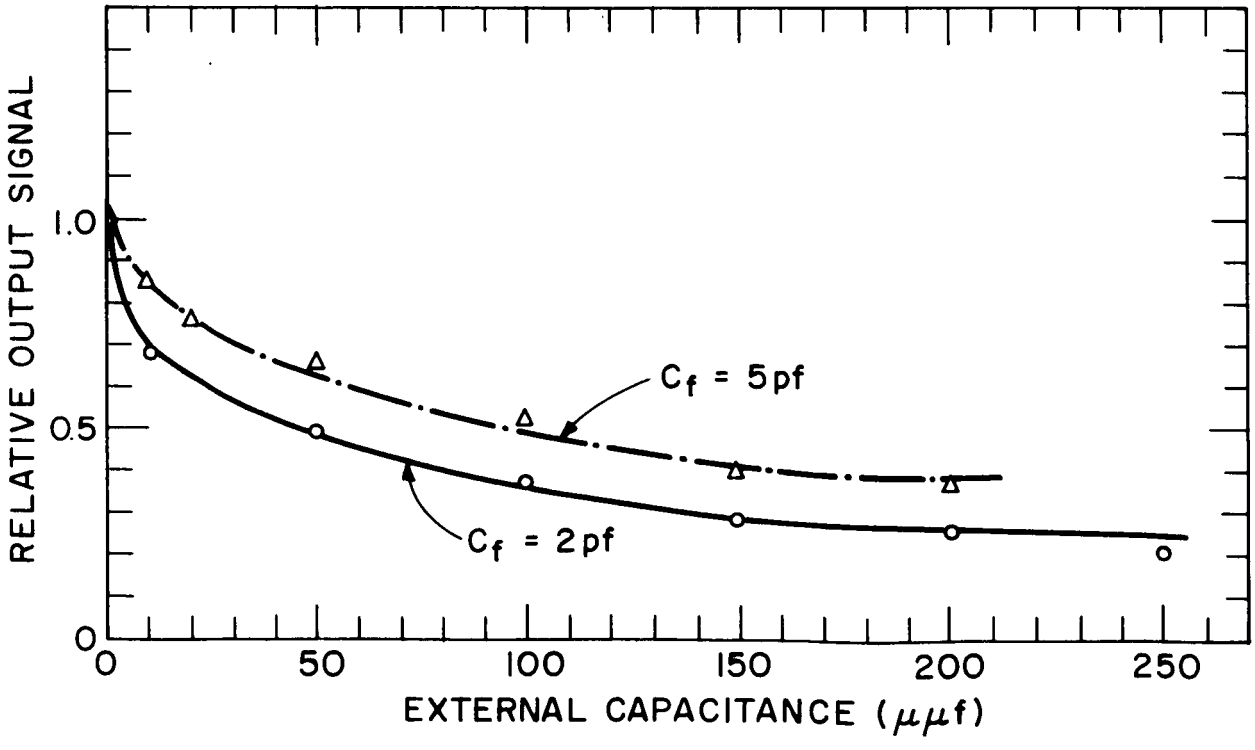

FIGURE 19

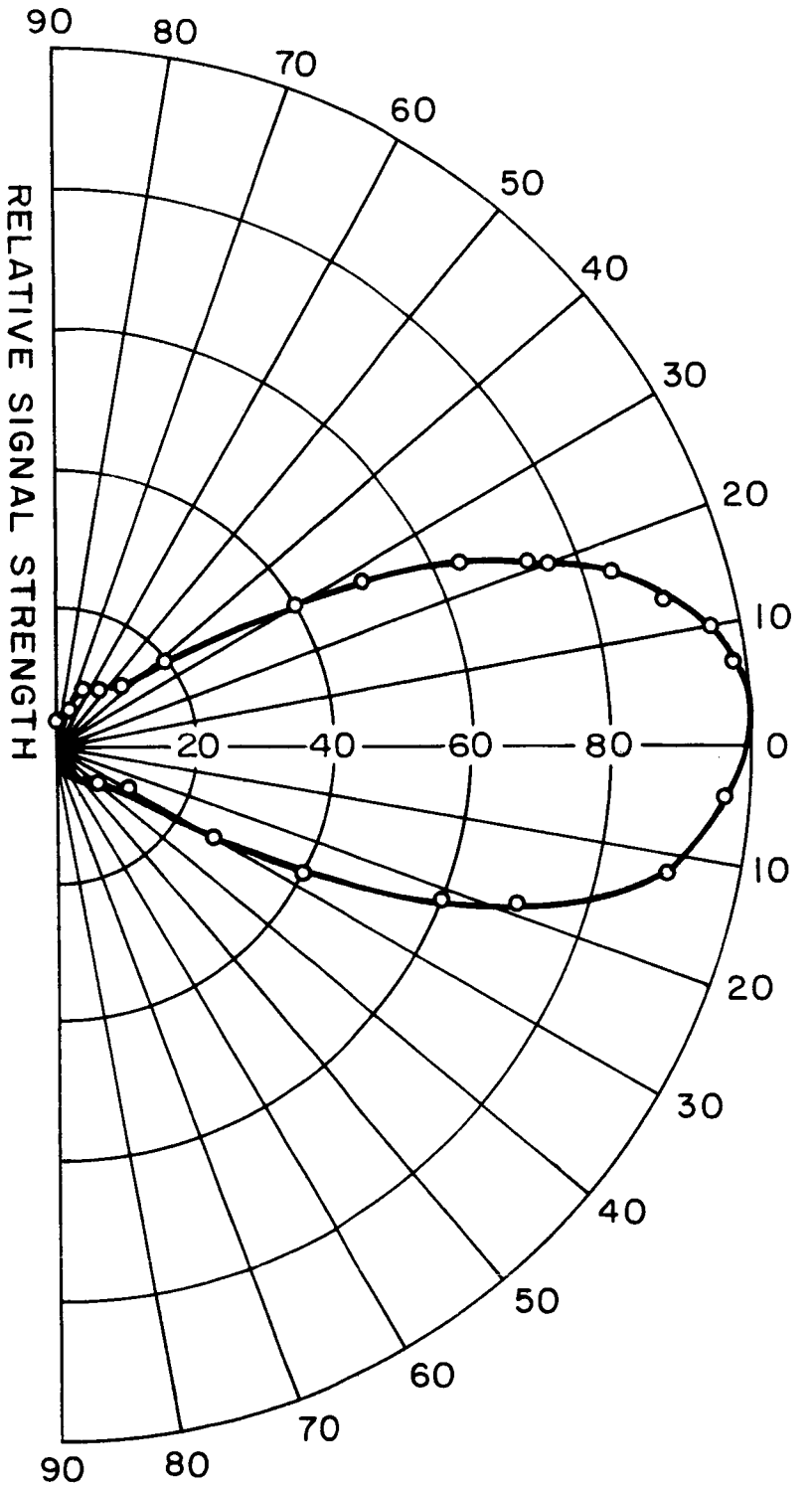

FIGURE 20

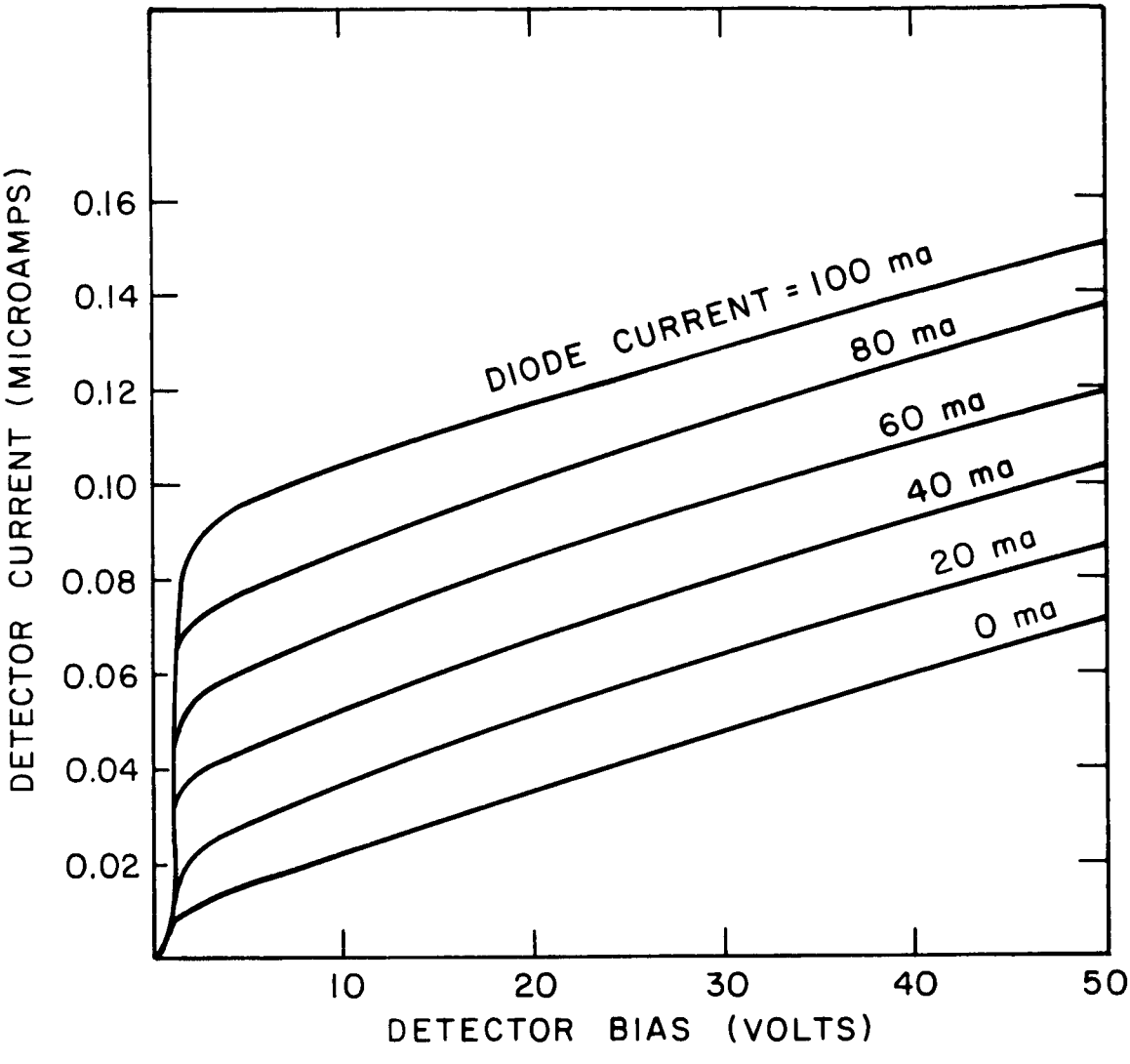
DETECTOR CURRENT (MICROAMPS)
0.16
0.14
0.12
0.10
0.08
0.06
0.04
0.02
DIODE CURRENT = 100 ma
80 ma
60 ma
40 ma
20 ma
0 ma
10
20
30
40
50
DETECTOR BIAS (VOLTS)

FIGURE 21

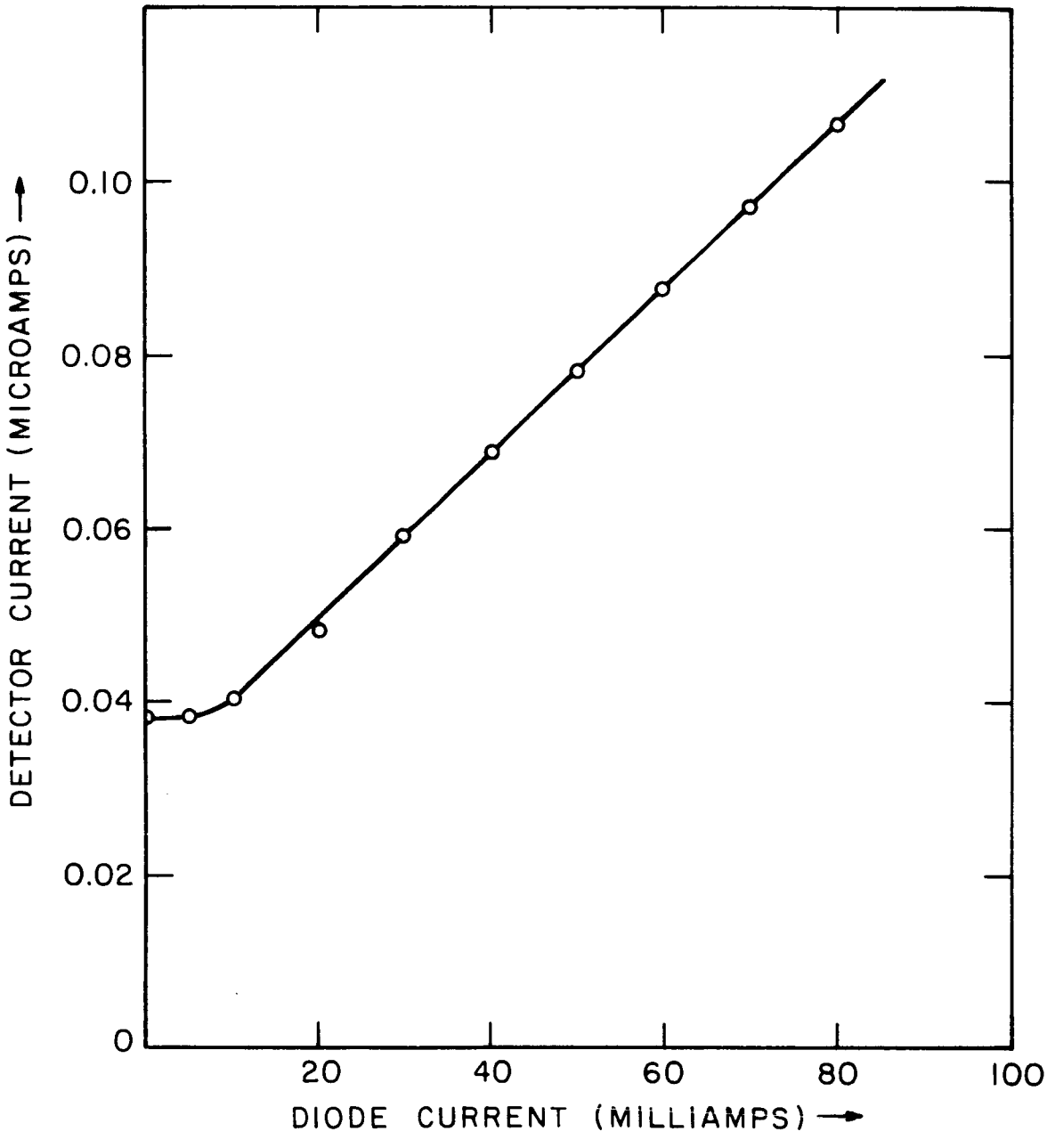
DETECTOR CURRENT (MICROAMPS) →
0.10
0.08
0.06
0.04
0.02
0
20
40
60
80
100
DIODE CURRENT (MILLIAMPS) →

FIGURE 22

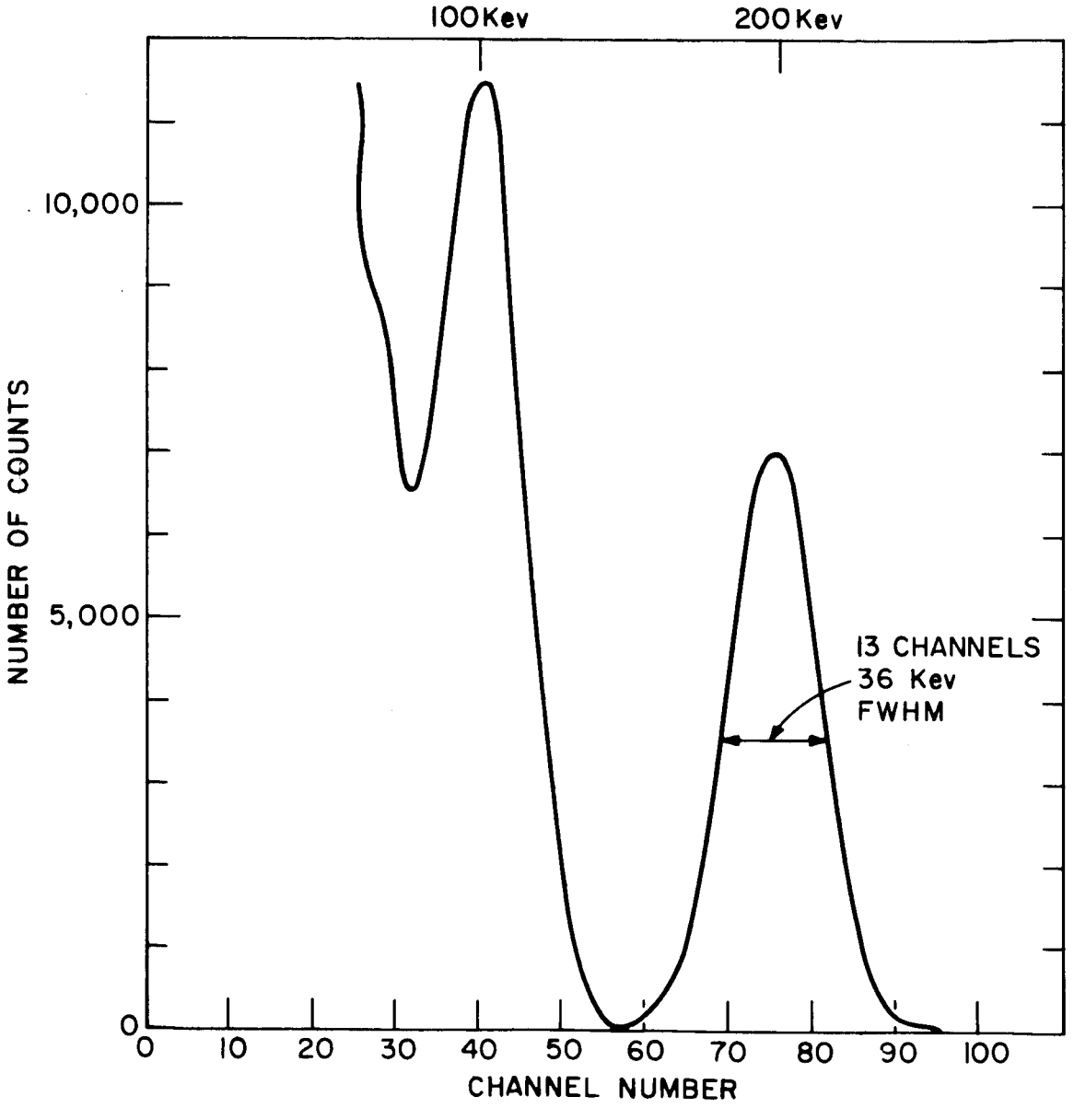
100Kev
200Kev
10,000
5,000
0
NUMBER OF COUNTS
13 CHANNELS
36 Kev
FWHM
0
10
20
30
40
50
60
70
80
90
100
CHANNEL NUMBER

FIGURE 23